AD-765 842

BLEACHABLE ABSORBER LASER AMPLIFIER AND
DETECTOR (BALAD)

James T. LaTourrette, et al

Polytechnic Institute of Brooklyn

Prepared for:

Rome Air Development Center
Defense Advanced Research Projects Agency

May 1973

BLEACHABLE ABSORBER LASER AMPLIFIER AND DETECTOR
(BALAD)

Polytechnic Institute of Brooklyn

Approved for public release;
distribution unlimited.

The views and conclusions contained in this document are those
of the authors and should not be interpreted as necessarily
representing the official policies, either expressed or implied,
of the Defense Advanced Research Projects Agency or the U. S.
Government.

Rome Air Development Center
Air Force Systems Command
Griffiss Air Force Base, New York

REPORT DOCUMENTATION PAGE	READ INSTRUCTIONS BEFORE COMPLETING FORM	
1. REPORT NUMBER RADC-TR-	2. GOVT ACCESSION NO.	3. RECIPIENT'S CATALOG NUMBER
4. TITLE (and Subtitle) Bleachable Absorber Laser Amplifier and Detector (BALAD)	5. TYPE OF REPORT & PERIOD COVERED Interim Report Jan 72 to Jul 72	
	6. PERFORMING ORG. REPORT NUMBER PIBEP-73-127	
7. AUTHOR(s) Jame T. LaTourrette and John Wilson	8. CONTRACT OR GRANT NUMBER(s) F30602-72-C-0245	
9. PERFORMING ORGANIZATION NAME AND ADDRESS Polytechnic Institue of Brooklyn Graduate Center Route 110, Farmingdale, NY 11735	10. PROGRAM ELEMENT, PROJECT, TASK AREA & WORK UNIT NUMBERS 12790011	
11. CONTROLLING OFFICE NAME AND ADDRESS RADC/OCTP GAFB/NY 13441	12. REPORT DATE	
	13. NUMBER OF PAGES 55 54	
14. MONITORING AGENCY NAME & ADDRESS(If different from Controlling Office)	15. SECURITY CLASS. (of this report) Unclassified	
	15a. DECLASSIFICATION/DOWNGRADING SCHEDULE NA	

16. DISTRIBUTION STATEMENT (of this Report)

Approved for public release. Distribution Unlimited.

17. DISTRIBUTION STATEMENT (of the abstract entered in Block 20, If different from Report)

18. SUPPLEMENTARY NOTES

19. KEY WORDS (Continue on reverse side if necessary and identify by block number)
Laser amplifier, Laser receiver, Laser detector, CO_2 laser, Xenon laser, Absorber, Bleachable absorber, Saturable absorber, Gaseous absorber, Optical filter, Sulfur hexafluoride, Optical waveguide, Optical radar, Optical communications, Wide-angle detector, Low-noise detector, Coherent detector, Narrow band filter, Spatial filter.

20. ABSTRACT (Continue on reverse side if necessary and identify by block number)
This report describes the continued development of the wide-angle, low noise BALAD receiver (Bleachable Absorber Laser Amplifier and Detector). The spatial and frequency resolution of a SF_6 saturable absorber in a 10.6 um BALAD configuration has been measured. The experimental results agree with the theoretical predictions. The components of a xenon-xenon 3.5 um BALAD system have been assembled, and experimental tests have been initiated. The theoretical analysis of the

DD FORM 1473 EDITION OF 1 NOV 65 IS OBSOLETE

Block 13 (Contd)

propagation of coherent optical pulses in resonant media has been extended
to three dimensions, but only preliminary results have been obtained.

BLEACHABLE ABSORBER LASER AMPLIFIER AND DETECTOR
(BALAD)

James T. LaTourrette
John Wilson

i

Title of Report   Bleachable Absorber Laser Amplifier
and Detector (BALAD)

PUBLICATION REVIEW

This report has been reviewed and is approved. For further technical information on this project, contact W. Quinn, RADC/OCTP/GAFB/NY 13441

Approved:

WILLIAM C. QUINN
Project Engineer/OCTP

Approved:

ALFRED W. PARKER
Assistant Chief, Techniques Branch
Surveillance & Control Division

ABSTRACT

This report describes the continued development of the wide-angle, low noise BALAD receiver (Bleachable Absorber Laser Amplifier and Detector). The spatial and frequency resolution of a SF_6 saturable absorber in a $10.6\mu m$ BALAD configuration has been measured. The experimental results agree with the theoretical predictions. The components of a Xenon-Xenon $3.5\mu m$ BALAD system have been assembled, and experimental tests have been initiated. The theoretical analysis of the propagation of coherent optical pulses in resonant media has been extended to three dimensions, but only preliminary results have been obtained.

TABLE OF CONTENTS

LIST OF FIGURES

1.0 SUMMARY

1.1 Objective

The objective of this contract is the investigation of Saturable Absorbers at 10.6μ and 3.5μ, and their application to BALAD receivers.

1.2 Background

In the BALAD (Bleachable Absorber Laser Amplifier and a Detector) concept, the gaseous absorber is designed to saturate at an average intensity above the amplified spontaneous emission. Thus, the spontaneous emission and other background light is absorbed. The bleachable gas acts as an optical squelch suppressing the background radiation which does not coincide with the signal beam in direction, polarization, frequency and time. In addition, the signal beam, being of somewhat higher intensity, is focused down on the absorber, "burns a hole" in it, and passes through with relatively little attention. Only light which is spacially coherent with the signal gets through to the detector.

During the first year's effort under Contract F30602-71-C-0024, a search was made for useful absorbers in the 10.6μ and 3.5μ ranges, and a design study was pursued. As a result, the gas SF_6 was found to possess adequate properties for the 10.6μ wavelength and Xenon was found to have very good properties at 3.5μ. Demonstration of the BALAD principle at 3.5μ with Xenon appears to be much more straightforward and considerably less costly at this time than a similar experiment at 10.6μ with SF_6. The present effort is a logical continuation of the work previously performed under Contract F30602-71-C-0024, and includes the areas defined in Tasks 4.1.1 thru 4.1.3.

1.3 Plan

The study and investigation for the development, design, test, and analysis of the concept of a Bleachable Absorber Laser Amplifier and Detector (BALAD) has been delineated into the following four tasks:

Task 4.1.1: Development of design techniques for the BALAD concept. In part this will involve refinement of the concepts developed under Contract F30602-71-C-0024.

Task 4.1.2: Develop techniques for filtering out radiation from all but the working line in the 10.6μ CO_2 laser amplifier and in amplifiers in the $3-5\mu$ spectral range with the objective of determining the optimum technique to be used in a BALAD receiver.

Task 4.1.3: Experimental demonstration of a BALAD receiver utilizing Xenon both as the absorbing and amplifying gases; in particular, using a pulse modulated Xenon oscillator as a source, measure and compare with theoretical predictions

the performance of the BALAD receiver as a function of input pulse energy, duration and direction of propagation with respect to the parameters: pulse energy amplification, amplification bandwidth, absorber filter bandwidth, field of view, absorber geometry, no detection and false detection error rates in the pulsed case, signal to noise ratio in the CW case.

Task 4.1.4: System Safety Analysis. In the conduct of design and fabrication of hardware a system safety analysis shall be performed and documented. These studies shall be in accordance with Paragraph 5.8.2.1 of MIL-STD-882 where applicable.

1.4 Technical Problems, Methodology, and Results

During this period, the Bleachable Absorber component of a CO_2-SF_6 BALAD system has been tested and the results are reported here. A Xenon-Xenon BALAD system has been assembled; but only preliminary tests have begun. The results obtained on this and the remaining tasks will be reported in the final report. The theoretical analysis of the propagation of a realistic optical pulse with limited transverse extent has progressed. Preliminary results indicate the existence of a strong focusing effect in the saturated absorber, which might yield a significant improvement in the design of a BALAD receiver. The following subsections summarize the developments in each of these topics.

1.4.1 Experimental Study of Components of a CO_2-SF_6 BALAD Receiver System

The heart of any BALAD system is the saturable absorber. In conjunction with associated optics, this element provides a filter or aperture, which passes the signal and blocks all noise components which are not coherent with the signal. Although the desired filter or aperture behavior is based on a firm theoretical basis, and the hole burned in the frequency spectrum has been observed, the existence of the "spatial hole" has not, in fact, been subjected to previous experimental test. The purpose of this task is to provide a conclusive experimental test of the BALAD concept. The experimental results were precisely in accord with theory. The "spatial hole" agreed with the expected "diffraction limited" minimum spot size and we have confirmed that the "hole" in the frequency spectrum agrees with the expected power broadened homogeneous linewidth. These results are detailed in Section 2.

1.4.2 Experimental Study of the Xenon-Xenon BALAD Receiver System

The assembly of the Xenon-Xenon BALAD receiver system is essentially complete. Preliminary results have been obtained with a 5mm diameter, 20cm long pure Xenon absorption cell. These results, compared with the previous results with a 10mm bore tube, indicate that the maximum absorption varies as (1/diameter). Discharge noise

2

has been a major problem, and may limit the usefulness of the Xenon-Xenon BALAD system. These results are discussed briefly in Section 3.0, and will be reported in detail in the final report.

1.4.3 Transverse and Spatial Evolution of Optical Pulses in a Saturated Absorber

The theoretical analysis of the propagation of an optical pulse in a saturated absorber has been significantly advanced. The analysis specifically treats the realistic case of a pulse of limited transverse dimensions. Preliminary results indicate the existence of a strong self-focusing effect which could result in a significant improvement in the design of a BALAD receiver. These results are discussed briefly in Section 4.0, and will be reported in detail in the final report.

1.5 Implications for the Department of Defense

The previous study[1] indicated that a BALAD receiver for $10.6\mu m$ CO_2 laser signals as reported in RADC-TR-72-313, is feasible for application in an optical radar. Its usefulness would be to detect a target of uncertain position. For example, the receiver could be remote from the transmitter. The BALAD receiver could also sensitively receive several separated signals simultaneously, or even an entire image. The spatial and spectral resolution of an SF_6 saturable absorber in a BALAD receiver has been experimentally verified.

A BALAD receiver utilizing Xenon gas could function in a shorter range but higher resolution optical radar than the CO_2 system. This wide-angle receiver also could be utilized in a lightweight secure communication system. Discharge noise in the Xenon absorber may limit the usefulness of the Xenon-Xenon BALAD system.

1.6 Implications for Further Research and Development

The difficulties encountered with the Xenon absorber discharge noise point up the need for further research to achieve quiet discharge conditions while achieving the desired high absorption coefficient.

The self focusing effect, indicated by the numerical analysis of the propagation of a spatially limited pulse in a saturated absorber should be investigated further. If the effect is sufficiently strong, it could result in a significant improvement in BALAD receiver design.

2.0 EXPERIMENTAL STUDY OF COMPONENTS OF A CO_2-SF_6 BALAD RECEIVER SYSTEM[2]

2.1 Introduction and Background

2.1.1 Laser Receiver Requirements

A gaseous saturable absorber may be of use in the construction of a low-noise, wide-angle laser receiver. Such a receiver would have advantages in a practical radar system. Since the target direction is initially unknown, the receiver must have sufficient field-of-view such that the solid angle of interest can be scanned with a reasonable number of transmitted pulses. The pulse energy returned by a distant target of small optical cross-section may be quite small, necessitating a sensitive receiver, with low noise, to insure satisfactory error rates.

Direct detection with a large-area detector can give the required field-of-view. However, thermal receiver noise, a less than perfect detector quantum efficiency, and the radiance of the sky result in poor noise characteristics. Heterodyne reception can be used to achieve excellent Signal to Noise ratios. However, it suffers from the following deficiencies: very limited field-of-view; excessive receiver complexity; rapid signal degradation in an imperfect atmosphere. A receiver which promises to have better characteristics as far as field-of-view, detectivity, and receiver complexity is the BALAD receiver[1].

2.1.2 The BALAD Receiver

The BALAD receiver (Bleachable Absorber Laser Receiver and Detector) consists of a high gain laser pre-amplifier, a bleachable (saturable) absorber, and a large-area detector as shown in Figure 1. The signal is directed through the laser amplifier section in which it is amplified along with spontaneous emission from the amplifier medium. The system parameters are adjusted so that the spontaneous emission intensity, upon entering the absorption cell, is insufficient to saturate the absorber. Therefore, the spontaneous emission noise (as well as all other background radiation) is absorbed. The signal, focused to a spot of somewhat higher intensity, saturates, or "burns a hole" in the absorbing medium and suffers much less attenuation. Spontaneous emission which is spatially and spectrally coherent with the signal also passes through with relatively little attenuation. However, this is the fundamental limiting noise for _any_ detection system.

The spectral selectivity results from the fact that in a Doppler-broadened medium, the signal will saturate that velocity group which is resonant with the signal field[3].

The spatial (angular) resolution results from the fact that the signal from an unresolved target, at least in an unperturbed atmosphere, will occupy only one spa-
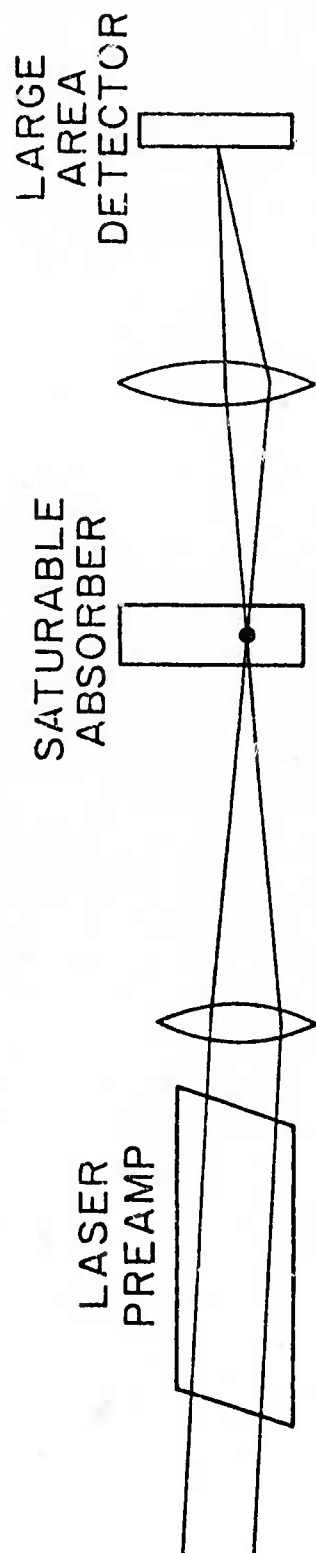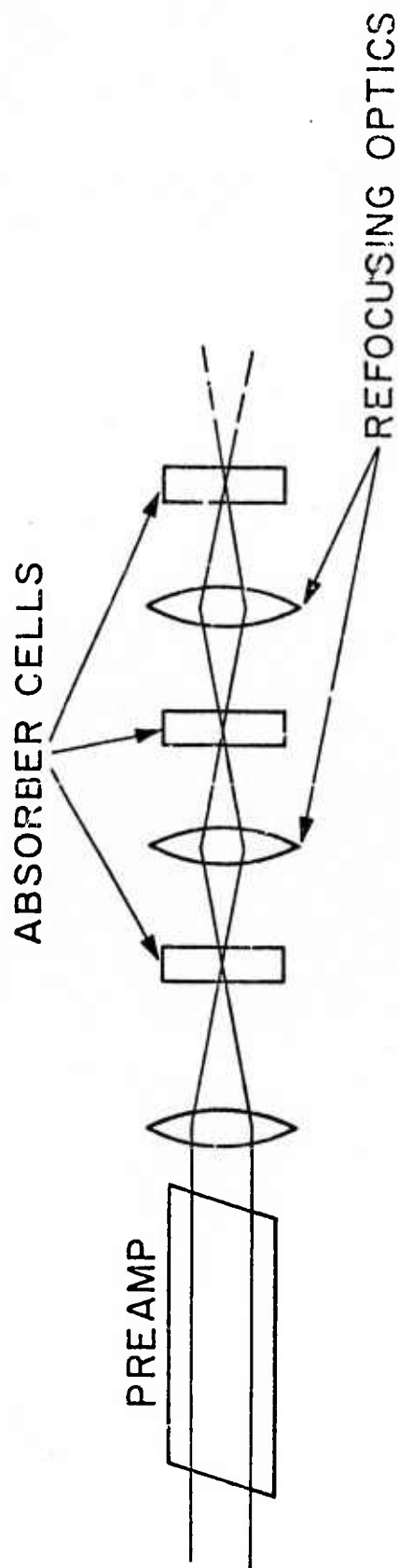
4

Fig. 1 - The BALAD Receiver

LASER PREAMP

SATURABLE ABSORBER

LARGE AREA DETECTOR

Figure 2 - A Practical BALAD Receiver

PREAMP

ABSORBER CELLS

REFOCUSING OPTICS

5

tial mode. For the purposes of this report, a spatial mode will be considered the diffraction-limited spot characteristic of the collection optics. If the spot size in the absorber is larger than the average diffusion length, there will be negligible cross-relaxation between spatial modes.

2.1.3 A Practical BALAD Receiver

The most promising laser/absorber combination is a CO_2 laser and sulfur hexafluoride (SF_6) as the absorber. The high efficiency, high power output, and usable gain of CO_2 as a laser medium, coupled with the transparency of the atmosphere at 10.6 microns make it an excellent choice for the laser/amplifier medium. Sulfur hexafluoride has a relatively high absorption coefficient, a low saturation intensity and absorption bands which overlap all interesting CO_2 laser transitions at room temperature.

Over the range of pressure of interest, the absorption coefficient is proportional to the number of absorbing molecules per unit volume, i.e., it is proportional to the pressure, p. The intensity to saturate the medium, on the other hand varies as p^2. The conflicting requirements lead to operation at low pressures with long cells in order that the required pre-amplifier gain will not be unreasonable.

Since it is essential to keep the medium well saturated by the signal beam, it is important to keep the beam diameter small in order that the intensity be as high as practical in the absorber. The actual receiver configuration may have to be shown in Figure 2, where the beam is periodically refocused down to a small spot in the absorber cells.

A typical arrangement might be to (somewhat arbitrarily) restrict the beam diameter to $\sqrt{2}$ of the minimum beam diameter (i.e., a factor of 2 in area). Alternative structures might use a "fly's eye" lens system or a bundle of optical waveguides to prevent the beam from respreading[1].

2.1.4 The SF_6 ν_3 Absorption

The SF_6 molecule is a symmetric rotor with the sulfur atom at the center of symmetry. It has several absorption bands in the infrared region, including the ν_3 band[4] at 947.9 cm^{-1}. Rotational line splitting causes many of the ν_3 absorption lines to overlap with CO_2 laser transitions. Of particular interest is the line which overlaps the P(18) transition in CO_2; its high absorption coefficient, closeness to the CO_2 line center, coupled with the high power output available from the laser on this transition, make it a good choice for this investigation. All calculations and measurements to follow assume operation on this line unless otherwise stated. Some of the characteristics of this absorption line which will be important for the purposes of analysis are as follows:

1. The absorption coefficient is a linear function of pressure, as was indicated earlier. Its value[5] per unit pressure at SF_6 line center is approximately $0.7 \, cm^{-1}$ $Torr^{-1}$ and the lineshape is Gaussian, consistent with Doppler-broadening[6].

2. It has been shown[5] that the saturation intensity is quadratic in A, the total rotational relaxation rate. At pressures where diffusion to the walls is negligible (above ~ 10 mTorr) the rotational relaxation is predominantly due to collisions. Since the collision rate is proportional to pressure, the saturation intensity varies as p^2. Its experimental value at 60 mTorr is $25 \pm 8 \, mW/cm^2$.[5]

3. The homogeneous lindwidth, $\Delta \nu_h$, at the pressure used in this experiment, is predominantly due to collisions and therefore is linear in p.

2.1.5 Objectives

The objective of this research was to investigate the performance of a BALAD receiver configuration. Toward this end, an experimental cell was constructed and incorporated into an arrangement of lasers and optics suitable for the measurement of various system parameters.

In particular, the spatial and spectral extent of the "hole," and the signal/noise attenuation will be measured and compared with the results predicted by the theory which will be presented and developed.

2.2 Theory

In this section, the theory of the BALAD receiver will be examined and in particular, expressions will be found to predict the angular discrimination, the spectral discrimination, and the extent to which incoherent noise will be attenuated below the signal. Throughout, the receiver configuration shall be assumed to be the "free-focus" configuration shown in Figure 1.

2.2.1 Angular Discrimination

Angular discrimination in the free-focus BALAD receiver is proportional to the physical size of the "hole" burned in the saturable absorber by the signal beam. The solid angle through which the hole is seen at the collection aperture is essentially the same solid angle through which noise will be able to enter and suffer the same relatively small attenuation as the signal.

A typical arrangement in a BALAD receiver might be to choose a cell length such that the beam will only diverge to $\sqrt{2}$ of its minimum diameter (see Figure 3). In order to estimate the beam size, some approximations will be made. The diffraction pattern of a plane wave passing through a circular lens, has, in the focal plane, a radial dependence of the form $J_1(r)/r$ where J_1 is the first order Bessel function of the first kind. After traveling through a saturable absorber, the anti-
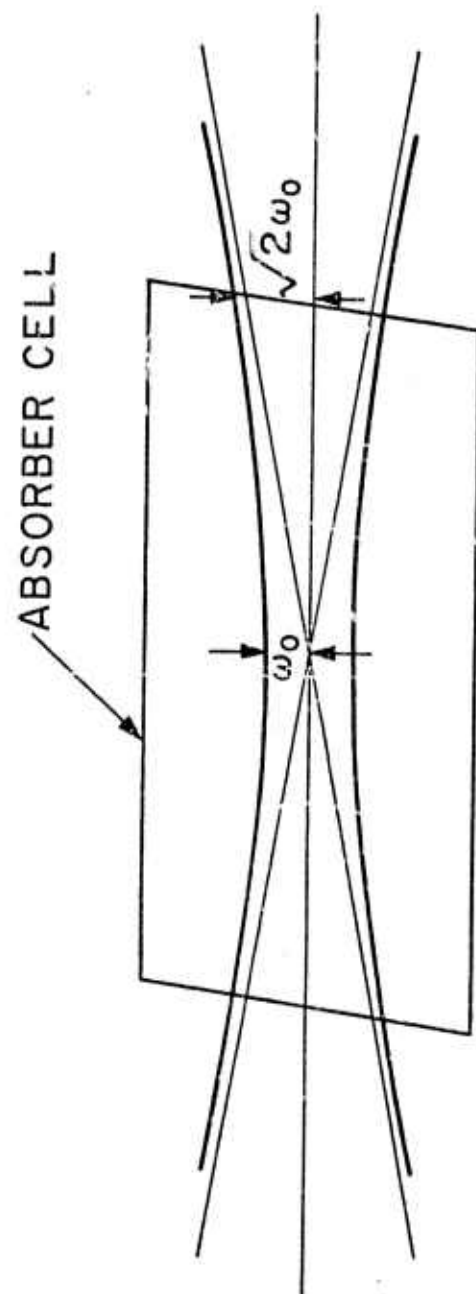
Fig. 3 - Beam Waist Shape

nodes of the radial function, except for the one at $r = 0$, will be attenuated away faster than the "main" lobe because of their less complete saturation of the absorption. This will give rise to a field which at least qualitatively appears to be Gaussian in radial dependence. A Gaussian field, near the focal point, can be well approximated by the confocal resonator theory of Boyd and Kogelnick[6]. The variation of the confocal beam radius, ω, with distance along the confocal axis is given by

$$\omega = \omega_o \left[1 + \left(\frac{z}{z_o}\right)^2 \right]^{\frac{1}{2}} \quad \text{where} \quad z_o = \frac{\pi \omega_o^2}{\lambda} . \tag{1}$$

The cross-sectional area of the beam clearly doubles when $z = z_o$. The length of the absorber cell is then restricted to $2z_o$, or

$$L = 2\pi \omega_o^2 .$$

The beam radius at the center of the cell, ω_o, can be taken, to a first approximation, to be the radius of the beam had the saturable absorber not been present. This is given by[*]

$$\omega_o = 1.22 \lambda \left(\frac{f}{D}\right) \quad \text{where} \quad \begin{array}{l} f \text{ is the focal length} \\ D \text{ is aperture diameter.} \end{array} \tag{2}$$

If the hole burned in the saturable absorber has this same radius, then the angular discrimination of the BALAD receiver is equal to the resolving power of the collection optics. It is important to note, however, the assumptions used to arrive at this result. First, there is no spatial mode-mixing in the off-focal-plane regions which two adjacent modes have in common. Second, diffusion and thermal convection effects, which would tend to carry saturated molecules from one mode to another, are negligible. Third, the beam diameter is not changed by the presence of the saturable absorber.

2.2.2 Signal and Noise Attenuation

In this section, expressions will be derived to predict the attenuation experienced by the saturating signal, and by noise which is incoherent, either spatially or spectrally with the signal. The ratio of the signal attenuation to the noise attenuation figures prominantly in the calculations to follow and shall be referred to as the "hole depth."

---

[*]This is actually the first zero of J_1.

9

2.2.2.1 The Saturable Absorber Hole Depth

The problem of finding the attenuation of an approximately confocal field propagating through a saturable absorber is not readily soluble because of the complication resulting from the non-uniform beam intensity and the variation of the beam radius with position in the cell. As a first approximation, the behavior of plane waves of uniform intensity will be treated.

The attenuation of plane waves of intensity I, traveling through an absorptive medium is described by

$$\frac{dI}{dz} = -\alpha I \qquad \text{where } \alpha \text{ is the absorption coefficient.} \qquad (3)$$

For the case of an inhomogeneously broadened medium, α is given by[6]

$$\alpha = \alpha_0 \left(1 + \frac{I}{I_s}\right)^{-\frac{1}{2}} \qquad (4)$$

where I_s is the saturation intensity, and α_0 is the unsaturated absorption coefficient. The resulting equation is separable, yielding

$$-\alpha_0 \, dz = \frac{\sqrt{1+s}}{s} \, ds \qquad \begin{array}{l}\text{where s is the normalized} \\ \text{intensity } I/I_s \, .\end{array} \qquad (5)$$

The problem was solved by Rigrod[7] and is included in Appendix A. The solution is

$$-\alpha_0 \ell = A(s) \Bigg|_{s_1}^{s_2} = \left\{\ln s + 2(1+s)^{\frac{1}{2}} + 2\ln(\sqrt{1+s}+1)\right\} \Bigg|_{s_1}^{s_2} \qquad (6)$$

where s_1 and s_2 are the input and output intensities respectively. The function A(s) was evaluated by computer in the range $0.1 \le s \le 500$ and is shown plotted in Figure 4. The signal attenuation can now be formally expressed as

$$\frac{s_2}{s_1} = \frac{A^{-1}\left[A(s_1) - \alpha_0 \ell\right]}{s_1} \, . \qquad (7)$$

The attenuation of noise which is not coherent with the signal, and itself is not sufficiently intense to saturate the absorber is $\exp(-\alpha_0 \ell)$. The ratio of the two is the hole depth, R

$$R = \frac{A^{-1}\left[A(s_1) - \alpha_0 \ell\right]}{s_1} \exp(\alpha_0 \ell) \, . \qquad (8)$$

10
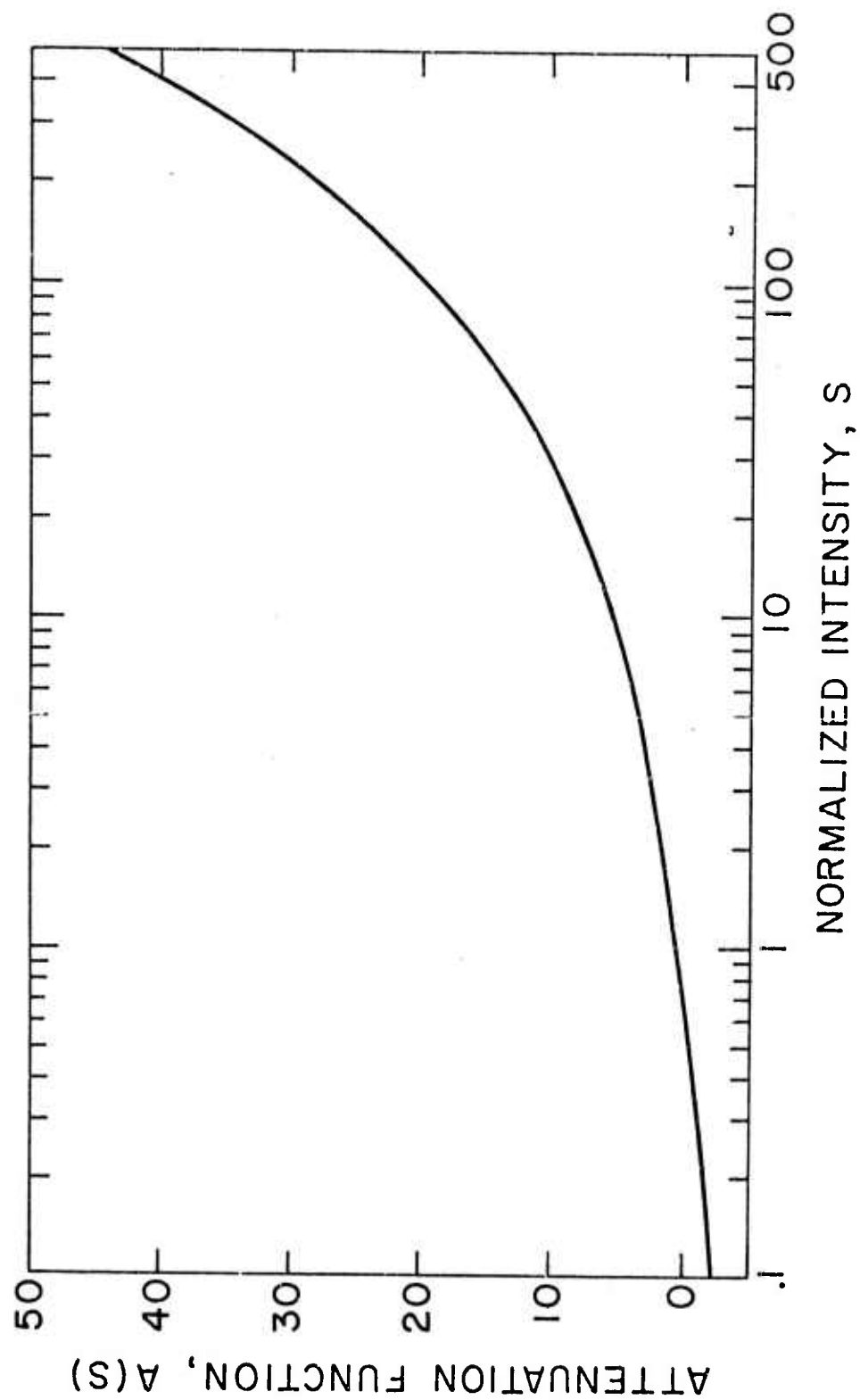
Fig. 4 - Attenuation Function; A(s)

The attenuation function, $A(s)$, may be inverted graphically or, as is done here, by the use of an iterative numerical procedure. According to Newton's Method, the $n + 1^{th}$ approximation to the root of the equation $f(x)$ is given by

$$x^{(n+1)} = x^{(n)} - \frac{f(x^{(n)})}{f'(x^{(n)})} .$$
(9)

In the case of the Attenuation function, $A(s)$, equation (9) becomes

$$s^{(n+1)} = s^{(n)} - \frac{A(s^{(n)}) - [A(s_1) - \alpha_o \ell]}{\sqrt{1 + s^{(n)}} / s^{(n)}} .$$
(10)

The procedure converges rapidly to the output intensity, s_2.

Because of the difficulty in varying the physical length of an experimental cell, it was decided to vary the parameter $\alpha_o \ell$ by changing the pressure. For an absorber of fixed length, with a given input intensity*, the hole depth as a function of pressure can be found. The absorption coefficient, α_o, and the saturation intensity, I_s, are explicitly given, in terms of pressure by

$$\alpha_o = \alpha' p$$
(11)

$$I_s = I' p^2$$
(12)

where I' and α' are the values at unit pressure. The input intensity $s_1 \equiv I/I_s$ is then

$$s_1 = I_1 / I' p^2 \equiv S_o / p^2$$
(13)

where S_o is the normalized input intensity at unit pressure. Equations (5), (6), (11), (12), and (13) can be combined and solved for R using the iteration of equation (10). This was done by computer and is shown plotted in Figure 10 for the values of α' and S_o given in sections, 2.3.2 and 2.3.3. The program is included in Appendix B.

2.2.2.2 The "Apparent" Hole Depth

Equation (7) allows the calculation of the attenuation of the signal and noise. Experimentally, these quantities can be measured by probing an absorption cell, through which the signal is propagating, with a weak, chopped test beam (see

---

*This refers to the un-normalized input intensity. The normalized intensity, s, varies with pressure through I_s.

12

Figure 7). The attenuation of the test beam, however, will not be the same as the signal because of the non-linearity of the medium.

If the frequency of the test beam is close enough to the signal beam, the two beams will interact with essentially the same group of absorbing molecules. The chopped test beam can then be considered[*] a small increment, Δs_1, added to the signal. This will give rise to a change in the output, Δs_2. The quantity $\Delta s_2 / \Delta s_1$ is then the small-signal, "a. c." (in analogy to circuit theory) attenuation of the medium. The ratio of its value with and without the signal present is defined as the "apparent" hold depth, H.

H can be found in the following manner in terms of the "true" hole depth, R.

$$A(s_2) = A(s_1) - \alpha_o \ell . \tag{14}$$

Taking finite differentials on both sides of equation (14) gives

$$A(s_2) \, \Delta s_2 = A(s_1) \, \Delta s_1 . \tag{15}$$

From equation (5)

$$A'(s) = \frac{(1 + s)^{\frac{1}{2}}}{s} . \tag{16}$$

Equations (15) and (16) are combined to give

$$\frac{\Delta s_2}{\Delta s_1} = \frac{s_2}{s_1} \left[\frac{1 + s_1}{1 + s_2} \right]^{\frac{1}{2}} . \tag{17}$$

A small fractional change in the input, $\Delta s_1 / s_1$, results in a larger fractional change in the output intensity than it would in the absence of the saturable absorber. This effect is related to the so-called "MARS" amplification[8] reported by Senitsky and Cutler.

In the absence of the strong, saturating signal, only the test beam is present. Then

$$\frac{\Delta s_2}{\Delta s_1} = \frac{s_2}{s_1} . \tag{18}$$

In the presence of the signal, $\Delta s_2 / \Delta s_1$ is given by equation (17). The apparent hole depth, H, is the ratio of equation (17) to (18) or

---

[*]This is so if the frequency difference is much smaller than the homogeneous band-width.

$$H = \frac{s_2^s / s_1^s}{s_2^o / s_1^o} \left[\frac{1 + s_1^s}{1 + s_2^s} \right]^{\frac{1}{2}} \qquad (19)$$

where the subscripts 1 and 2 refer to the input and output, respectively, and the superscripts s and o refer to with and without the saturating signal present. The first bracketed quantity in equation (19) can be recognized as R, the ratio of saturated to unsaturated attenuation. Equation (19) can be re-written as

$$H = R \left[\frac{1 + s_1^s}{1 + s_2^s} \right]^{\frac{1}{2}} \qquad (20)$$

H, which is implicitly a function of pressure, has been plotted in Figure 10.

2.2.2.3 Parametric Amplification Effects

Section 2.2.2.1 concerned itself with the attenuation of the signal, and that of noise which is totally incoherent, either spatially or spectrally, with the signal. There remains the question of what happens to noise which is spatially coincident with the signal, and is at (or near) the frequency of the signal.

It is reasonable to assume that some type of parametric effect does occur for noise which is at or near the signal frequency. In particular, some "MARS"-type amplification would be expected.

"MARS" amplification for an inhomogeneously broadened line, at a frequency offset from the "pump" is a very difficult problem and will not be attempted here. It is possible, however, to make some qualitative observations about this effect. At frequencies far from the "pump" (i. e., the signal), the effect should vanish since the two beams would be interacting with totally different groups of molecules. Conversely, for a small enough band about the signal frequency, assumed to be the homogeneous bandwidth, the amplification should be approximately constant.

For noise in that bandwidth (centered on the signal frequency) over which the parametric interaction can be regarded as constant, some quantitative treatment is possible. Over this bandwidth, the noise (CO_2 spontaneous emission or sky radiance) can be regarded as white. Hence, it can be represented by in-phase and quadrature field components whose amplitudes have a zero-mean, gaussian distribution[9], or equivalently, by AM and FM sidebands*. The quadrature (FM) component acts to vary the frequency, However, over this small frequency range, the medium is insensitive to frequency. The in-phase (AM) component, on the other hand, produces variations in the amplitude (and intensity) of the signal. The be-

---

*This assumes noise small compared to signal[1].

havior of the system to small variations in signal was discussed in section 2.2.2.2, the result being

$$\frac{\Delta s_2}{s_2} = \frac{\Delta s_1}{s_1} \left[\frac{1 + s_1}{1 + s_2} \right]^{\frac{1}{2}} \quad \ldots\ldots \text{ c. f. equation (17).} \tag{21}$$

Combining equations (20) and (21) yields

$$\frac{\Delta s_2}{s_2} = \frac{\Delta s_1}{s_1} \left(\frac{H}{R} \right). \tag{22}$$

It is shown in Appendix D that for this case (i. e., for noise which can be regarded coherent with the signal), the output signal to noise ratio is given by

$$\left(\frac{S}{N} \right)_2 = \left(\frac{S}{N} \right)_1 \left[\frac{R^2}{H^2} \right] \tag{23}$$

where S and N are the detected signal and noise powers respectively. For noise which is totally incoherent with the signal, the output S/N ratio is given by

$$\left(\frac{S}{N} \right)_2 = \left(\frac{S}{N} \right)_1 \left[R^2 \right]. \tag{24}$$

Therefore, for incoherent noise, the S/N ratio is increased (by the saturable absorber) by the factor R^2, while for approximately coherent noise it is degraded by the factor R^2/H^2 (less than unity).

In an optimized system, some value of R would be chosen for which the signal-to-(total) noise ratio would be maximized.

2.2.3 Spectral Discrimination

In this section, the results obtained in section 2.2.2, particularly equations (5) and (6), will be modified to include frequency in order to calculate the spectral width of the "hole." The spectral width of the hole is important because the amount of noise reaching the detector (neglecting parametric effects) is directly proportional to the effective "passband" of the saturable absorber.

The spectral response of the system will be evaluated using the assumption that the absorption coefficient can be considered to be a linear superposition of the absorption by the various classes (velocity groups) of absorbing molecules. Furthermore, it will be assumed that the homogeneous molecular response bandwidth, $\Delta \nu_h$, is much smaller than the full Doppler width, or equivalently, that the popu-

lation distribution can be regarded as approximately constant over several homogeneous bandwidths.

In order to determine the relevant characteristics of the hole, it is necessary to examine the mechanism of hole-burning. When a photon is absorbed by a molecule within a given velocity-group, that molecule is no longer available for absorption and the number of absorbing molecules in that velocity-group is decreased. This leads to a "hole" being burned in the velocity-group population distribution near the field frequency (i.e., where the field most strongly couples to the absorbing molecules).

The absorption at frequency ν by molecules belonging to the class ξ is directly proportional to the homogeneous lineshape factor, $g^{\xi}(\nu)$. For a collision-broadened line, the homogeneous lineshape is Lorentzian[3]

$$g^{\xi}(\nu) = \frac{\Delta \nu_h / 2\pi}{(\nu - \nu_{\xi})^2 + (\Delta \nu_{h'} 2)^2} \tag{25}$$

where $\Delta \nu_h$ is the full spectral width at half-maximum (FWHM), and ν_{ξ} is the center frequency for absorption by molecules of class.

The total rate of absorption (for a field at ν) is the sum of the contributions of each of the velocity-groups, in effect, a convolution of the homogeneous response function (the lineshape) with the velocity-group population distribution. The population distribution has been assumed to be approximately constant, except for the "hole" burned around the field frequency. The shape of the hole can be shown[6] to be given by an expression identical to equation (25) except that $\Delta \nu_h$ is replaced by $\Delta \nu_p$, the spectral width of the hole in the velocity distribution, given by

$$\Delta \nu_p = \Delta \nu_h (1 + s)^{\frac{1}{2}}. \tag{26}$$

The total rate of absorption is then given by the convolution of one Lorentzian (of width $\Delta \nu_h$) with a term which is the sum of a constant and another Lorentzian (of width $\Delta \nu_p$). The result of the latter term is also Lorentzian with a width equal to the sum of the two widths. That is, the spectral width of the hole in the absorption distribution, $\Delta \nu_a$, is given by

$$\Delta \nu_a = \Delta \nu_h + \Delta \nu_p = \Delta \nu_h [1 + (1 + s)^{\frac{1}{2}}]. \tag{27}$$

At the field frequency, the absorption coefficient is reduced by a factor of $(1 + s)^{\frac{1}{2}}$ as seen in equation (4). Knowing the depth, width and shape of the hole,

from equations (4), (27) and (25) respectively, the absorption coefficient can be
explicitly written in terms of frequency and intensity.

$$\alpha(\nu, s) = \alpha_o - \left[\alpha_o - \frac{\alpha_o}{(1-s)^{\frac{1}{2}}} \right] g(\nu) \tag{28}$$

$$= \alpha_o \left\{ 1 - \left[1 - \frac{1}{(1+s)^{\frac{1}{2}}} \right] \left(\frac{1}{1+x^2} \right) \right\} \tag{29}$$

where

$$x \equiv \frac{\nu - \nu_o}{\Delta \nu_h / 2} \left[\frac{1}{1 + (1+s)^{\frac{1}{2}}} \right] \tag{30}$$

and ν_o is the field frequency. The absorption coefficient is plotted vs. frequency
in Figure 5.

Equation (29) may be simplified to

$$\alpha(\nu, s) = \alpha_o \left[\frac{x^2 + \frac{1}{(1+s)^{\frac{1}{2}}}}{x^2 + 1} \right] . \tag{31}$$

By defining δ as the frequency deviation normalized to the homogeneous half-
width, the intensity dependence may be explicitly included

$$\frac{\alpha(\nu, s)}{\alpha_o} = \frac{\left[\frac{\delta}{1 + (1+s)^{\frac{1}{2}}} \right]^2 + \frac{1}{(1+s)^{\frac{1}{2}}}}{\left[\frac{\delta}{1 + (1+s)^{\frac{1}{2}}} \right]^2 + 1} \tag{32}$$

where

$$\delta = \frac{\nu - \nu_o}{\Delta \nu_h / 2} .$$

Equation (32) can be rearranged to

$$\frac{\alpha(\nu, s)}{\alpha_o} = \left[\frac{1}{(1+s)^{\frac{1}{2}}} \right] \left[\frac{s + 2 + 2(1+s)^{\frac{1}{2}} + \delta^2 (1+s)^{\frac{1}{2}}}{s + 2 + 2(1+s)^{\frac{1}{2}} + \delta^2} \right] . \tag{33}$$

Equation (33) gives the absorption coefficient vs. frequency for a saturable absor-
ber through which a strong saturating signal is propagating. If such a field is
propagating in the presence of noise, that noise which is close in frequency to the
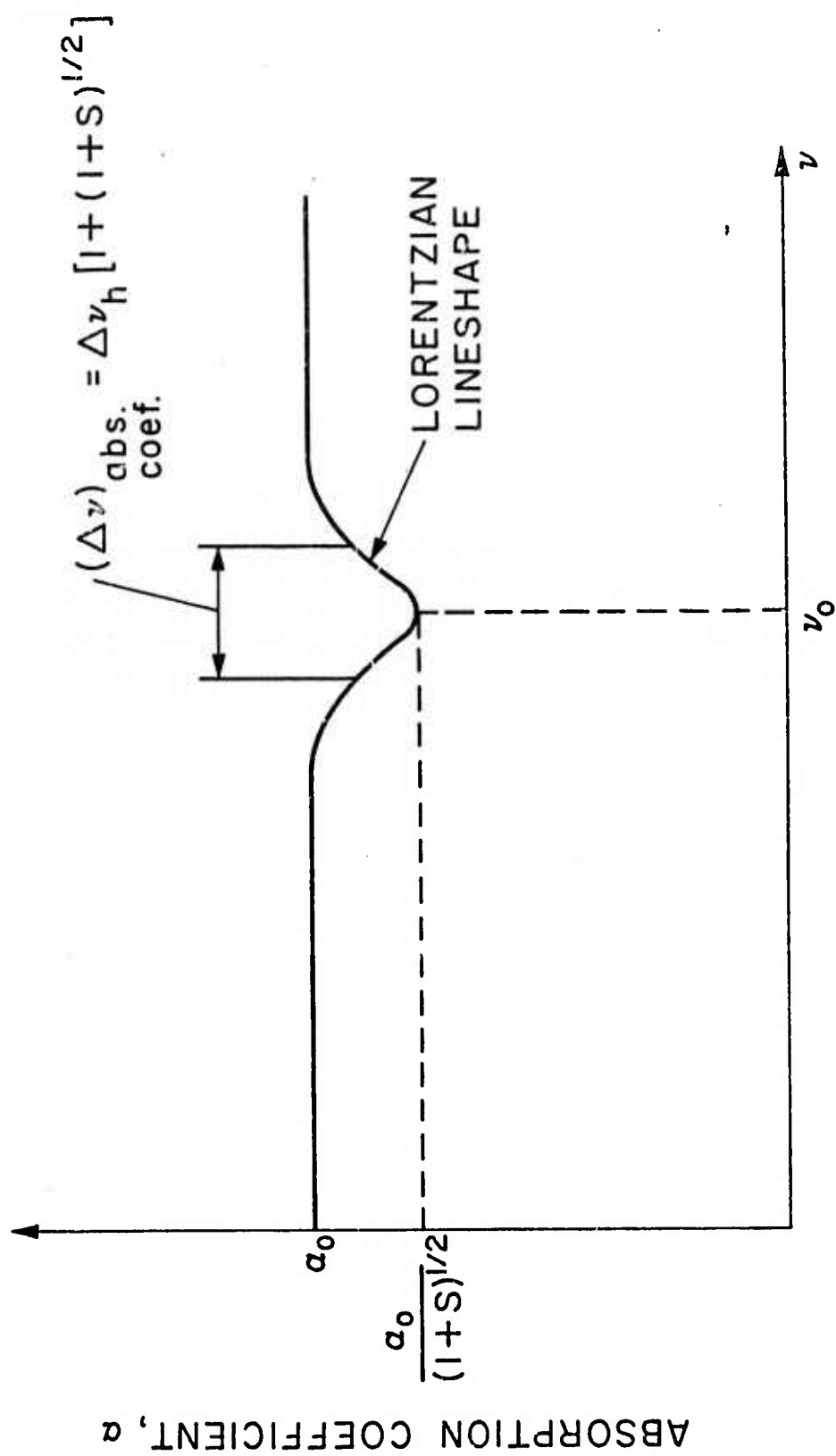saturating signal will suffer somewhat less than the unsaturated attenuation even

Fig. 5 - The Hole in the Absorption Coefficient

18

though that noise may be of insufficient intensity to saturate the medium itself.

In order to treat the problem of a small-signal field propagating through the absorber, it will be assumed that the saturation of the medium is the sole result of the intensity of the strong signal, i. e., the small-signal does not add to the saturation. This assumption neglects any parametric interactions which would be present and makes the problem a linear one. The propagation of the small-signal field is then described by

$$\frac{du}{dz} = -\alpha(\nu, s)u \tag{34}$$

where u is the normalized intensity of the small-signal field. Equation (34) can be written using the chain rule as

$$\frac{du}{u} = -\alpha(\nu, s) \, dz = -\alpha(\nu, s) \frac{dz}{ds} \, ds . \tag{35}$$

From equation (5)

$$\frac{ds}{dz} = -\alpha_o \left[\frac{s}{(1+s)^{\frac{1}{2}}} \right] . \tag{36}$$

When equations (33) and (36) are inserted into equation (35), the result is

$$\frac{du}{u} = \left[\frac{((1+s)^{\frac{1}{2}}+1)^2 + \delta^2 (1+s)^{\frac{1}{2}}}{((1+s)^2+1)^2 + \delta^2} \right] \frac{ds}{s} . \tag{37}$$

This can be integrated exactly (shown in Appendix A) with the result

$$u_2 = u_1 e^{\phi(s_2) - \phi(s_1)} \tag{38}$$

where the subscripts 1 and 2 denote input and output respectively and $\phi(s)$ is given by

$$\phi(s) = \ln s + \ln \left[\frac{(r+1)^2 + \delta^2}{(r+1)^2} \right] + 2\delta \tan^{-1} \left[\frac{r+1}{\delta} \right] \tag{39}$$

where $\qquad\qquad\qquad\qquad r \equiv (1+s)^{\frac{1}{2}} .$

As was indicated in section 2. 2. 2, it is convenient, in the experimental situation

to use a cell of fixed length and to vary the pressure. Using the parameters given in sections 2.3.2 and 2.3.3, the small-signal attenuation, given by equations (38) and (39) has been plotted in Figure 6. The fact that the homogeneous linewidth, $\Delta \nu_h$, is pressure-broadened through collisions is included so that the horizontal axis in Figure 6 can be read to be (within a constant factor) the actual frequency deviation in MHz.

2.3 Experiments and Results

In this section, the experiments performed as part of this research are described, as well as the apparatus and the experimental set-up. The results are compared with the theoretical predictions of Section 2.2.

2.3.1 Experimental Set-up

The set-up is shown in Figure 7. Laser 1 was operated in a folded confocal configuration. The reflectors were spaced 67 cm. apart and the spacing could be adjusted with a micrometer screw for gross length adjustments. One of the mirrors was also mounted on a piezoelectric transducer to provide for electrically tuning the cavity through length change. Laser 2 was also operated in a folded confocal configuration. However, this laser incorporated a diffraction grating as one of its feedback mirrors making it possible to select and tune across any CO_2 transition desired. It also had a piezoelectric transducer for electrical cavity length adjustment.

Both lasers were operated with gas fills of 1 Torr Xe: 2 Torr CO_2: 4 Torr N_2: 8 Torr He. The lasers both had a power output of approximately 1 watt CW when driven by 12 ma. constant-current supplies. The plasma tubes had 1 cm. bores and had NaCl windows affixed to each end.

The reflection optics shown are all first-surface aluminized mirrors and all refractive optics were AR-coated Germanium.

The absorption cell, which was made of glass, had an inside diameter of 2.2 cm. and a length of 17.5 cm. The windows were of BaF_2 and were cemented onto the cell ends. The cell was mounted in a cradle which could be mounted on a standard triangular optical bench and was connected to the gas-handling station using copper tubing. The SF_6 pressure was monitored using a Consolidated Vacuum Corporation Type GMS-140 vacuum gauge which was initially calibrated against an MKS Baratron capacitance manometer.

In order to synchronously detect the output of laser 2 in the presence of the other laser's output and noise, the output beam was chopped by a mechanical chopper wheel at approximately 220 Hz. The output was also passed through a dimethyl ether attenuator cell to provide for a continuously adjustable attenuation of the signal.
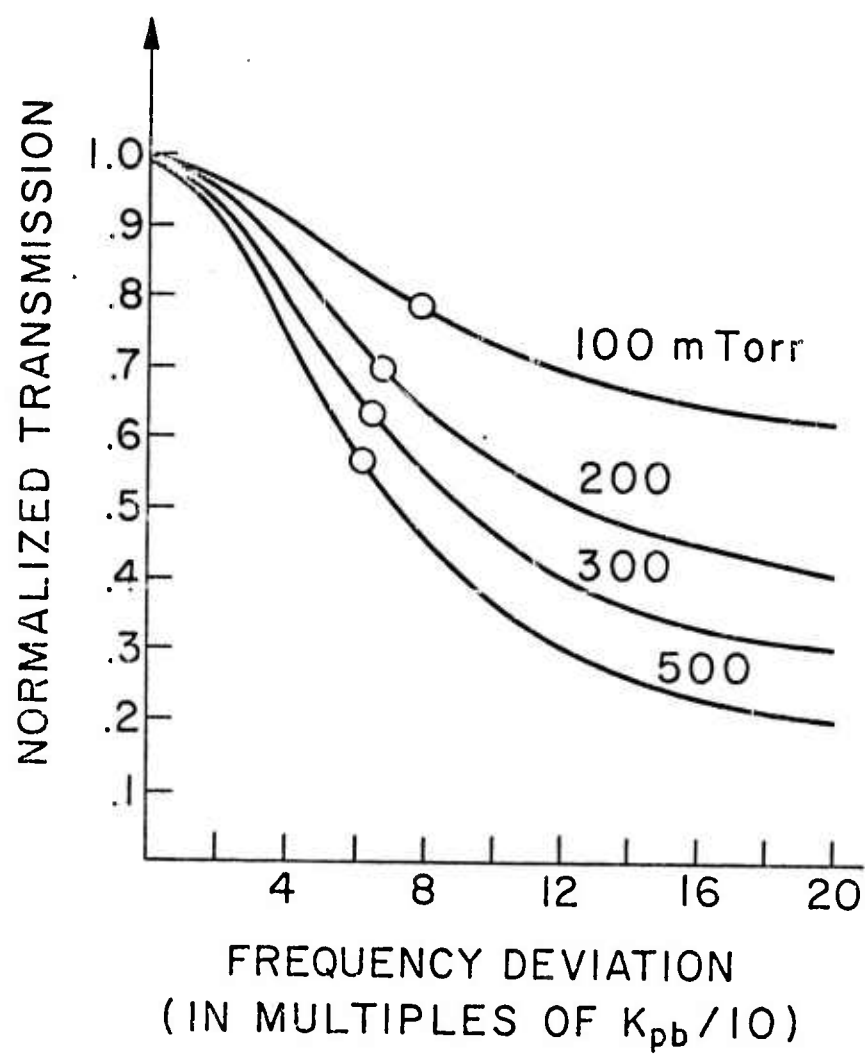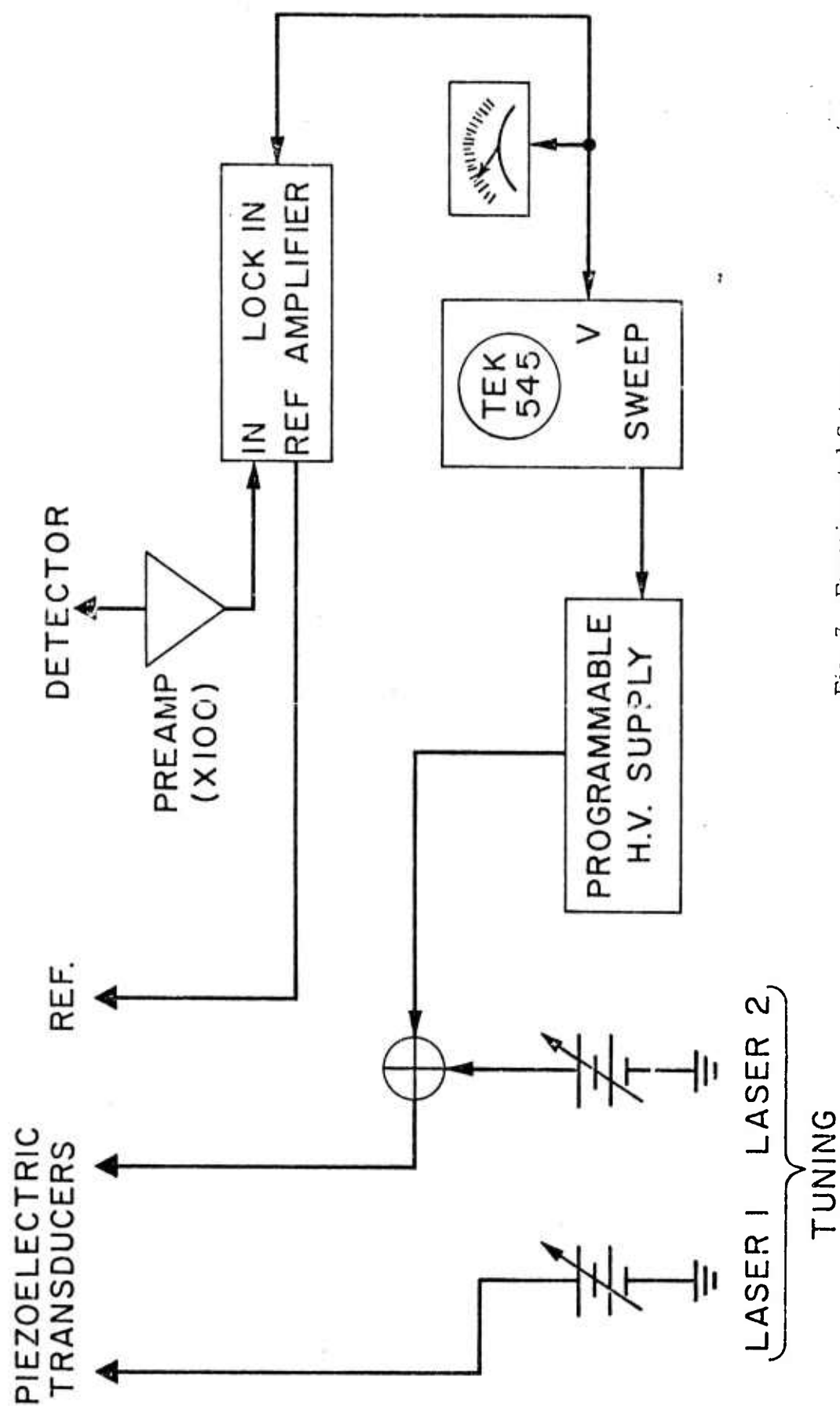
20

Fig. 6   Theoretical Hole Shapes

Fig. 7 Experimental Set-up

The signal was detected by a Philco GPC-215 Ge:Au detector and was amplified by a solid state preamp with a gain of $\approx$ 100 and a bandwidth of $\approx$ 100 kHz. The signal was then either displayed on a Tektronix 545 oscilloscope or passed through a Princeton Applied Research JB-5 Lock-in Amplifier. The synchronously detected signal was displayed on either the oscilloscope or a calibrated milliammeter. The total power through the aperture could also be measured using an Eppley thermopile. The sweep voltage for laser 2 was obtained from a Kepco Labs programmable high-voltage power supply which was programmed with the oscilloscope sweep output voltage.

2. 3. 2 Determination of Saturation Intensity

In order to determine the saturation intensity, the beam from laser 1 was blocked and the iris aperture was set at 4. 7 mm., appropriate for the length of the cell (see section 2. 3. 4). The SF_6 pressure was adjusted to 200 mTorr and the attenuation of the chopped signal (from laser 2) was measured for several values of input power. The input power equivalent to a normalized intensity of unity was found to be equal to approximately 1. 77 mW. by curve fitting of the data to equation (6) as shown in Figure 8.

The radius of the spot into which this power is focused is given by equation (2)

$$\omega_o = 1.22 \, \lambda \left(\frac{f}{D}\right).$$

The spot area is then $\pi \omega_o^2$ or .0092 cm^2. This would yield an intensity in the spot of 200 mW/cm^2, (assuming a uniform intensity across the spot).

Using equation (12), the saturation intensity at unit pressure, I', would be $5 \pm .5$ W/cm^2. At 60 mTorr, the saturation intensity would then be 18 mW/cm^2. This agrees well with the value (at 60 mTorr) obtained by Rabinowitz[5] which was 25 ± 8 mW/cm^2.

When the output of laser 1 was unblocked, adjusted to the same transition, and measured, it was found to produce an intensity within the cell which was 78 times the saturation intensity at 200 mTorr pressure. The value of S_o in equation (13) can then be found to be $3.12 \pm .3$.

The chief source of error was probably the assumption that the entire complex geometric situation could be approximated by a simple circular spot of uniform intensity and constant area.

2. 3. 3 Determination of the Absorption Coefficient

The absorption coefficient for any given SF_6 transition is a function of the frequency at which measurements are made. Specifically, it varies with frequency
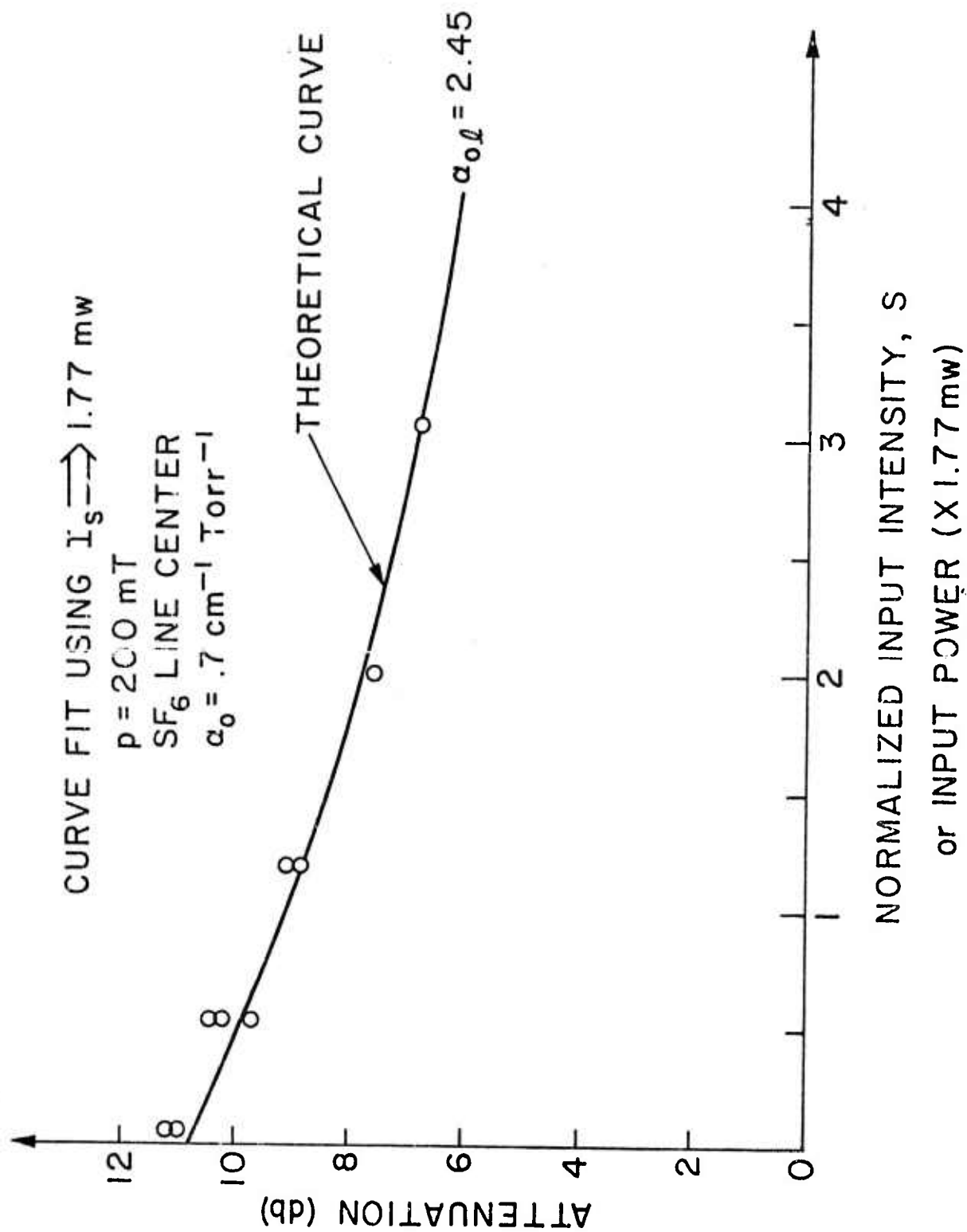
Fig. 8 Saturation Intensity Curve Fitting

in a gaussian manner (consistent with Doppler broadening).

The experiments which follow were all carried out at a frequency estimated to be $\approx$ 15 MHz. below the SF_6 line center. This was done because at the SF_6 line center, the P(18) CO_2 laser transition drops off rapidly with increasing frequency. Since the lasers were unstabilized, small frequency drifts would occur and cause significant variations in output power. These variations would make accurate, repeatable measurements difficult. At the frequency chosen for the experiments, the laser mode is essentially flat, making its output power relatively insensitive to small frequency changes.

The value of the absorption coefficient (per unit pressure) at the center of the SF_6 line overlapping the CO_2 P(18) transition is approximately 0.7 $cm^{-1}Torr^{-1}$. Since the full Doppler width for SF_6 at $300^{O}K$ is very nearly 30 MHz., the absorption coefficient at a frequency 15 MHz. away from line center is reduced by a factor of 2, that is, the value of α' in equation (11) is approximately 0.35 $cm^{-1}Torr^{-1}$. This agrees well with the value obtained through direct measurement of the attenuation of a small signal through the absorber.

2.3.4 Angular Discrimination

The angular discrimination, as defined in section 2.2.1, was measured as follows: The outputs of both lasers were unblocked and the pressure in the SF_6 absorption cell was set to approximately 200 mTorr. The iris diameter was set to 4.7 mm. which was determined by the requirement that the beam area must not increase by more than a factor of 2 from the center of the absorption cell to the windows (refer to equation (1)). The radius of the spot at the center of the cell can be calculated using equation (2) to be 0.54 mm. using a value of 20 cm. for the lens' focal length. The output of laser 2 was chopped and synchronously detected and adjusted to the minimum intensity necessary to give satisfactory readings. The angular orientation of the small-signal beam (laser 2) with respect to the strong beam, was then varied using a micrometer screw incorporated into the beam splitter mount. The intensity of the chopped signal reaching the detector was recorded for several values of angular displacement and is shown plotted in Figure 9. The frequency of the signal was periodically adjusted to insure that the frequencies of the two beams were held together.

The results of this procedure show that the observed hole size compares favorably with the calculated theoretical hole size.

2.3.5 Large and Small-signal Attenuation

The attenuation of a strong saturating field propagating through the SF_6 can be measured directly, or, as was done here, by probing the saturated medium with
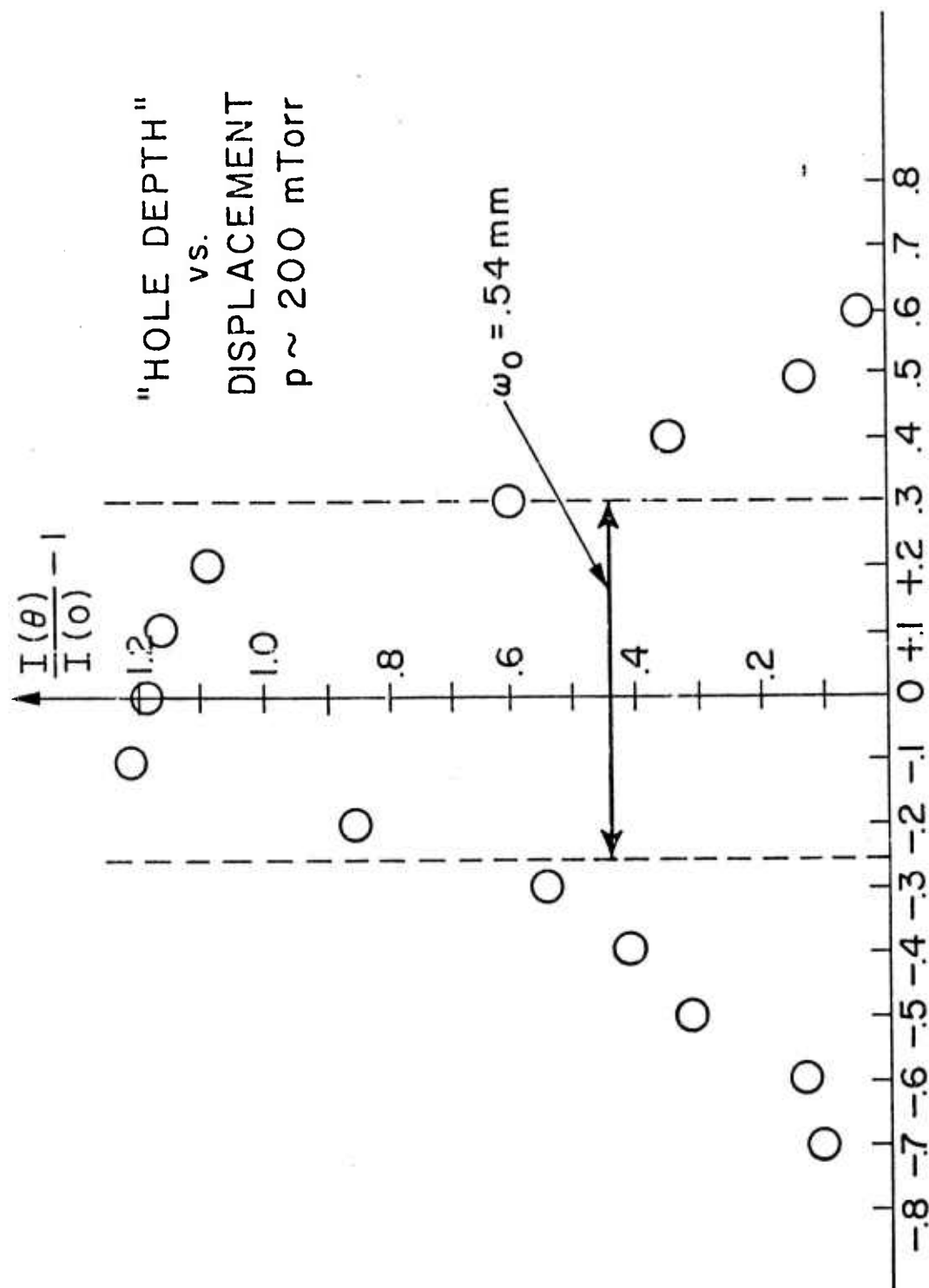
Fig. 9 Angular Discrimination

a weak, non-saturating, modulated test-beam.

The outputs of both lasers were directed through the absorption cell in the set-up shown in Figure 7 and the angular alignment was adjusted so that the two beams were exactly coincident within the cell. The lasers were tuned to the proper point on the P(18) line and laser 2 was adjusted to the minimum intensity necessary to give satisfactory results. The pressure was set to the desired value, and the frequency of laser 2 was adjusted to that of laser 1. The intensity of the chopped signal reaching the detector was measured using the lock-in amplifier and recorded. Next, the (saturating) beam from laser 1 was blocked and the amount of signal was again measured and recorded. The ratio of the two values is the "apparent" hole depth, H, as defined in section 2.2.2.2. The results of these measurements (at various pressures in the range 100-500 mTorr) are shown plotted in Figure 10 along with the theoretical predictions using the theory of section 2.2.2.2. The fit is quite good, and again the chief source of error is probably the assumptions concerning the geometry of the beam.

2.3.6 Spectral Discrimination

In order to measure the spectral extent of the hole, laser 1's output was blocked, and laser 2 was adjusted to the minimum usable level. A low-frequency sweep voltage was applied to the piezoelectric element used to tune laser 2. The sweep voltage varied in linear manner from zero to $\approx$ 450 v. The amplified output of the detector was displayed on the oscilloscope and is shown in Figure 11. The D.C. bias on the piezoelectric element was varied to shift the swept laser output pattern on the oscilloscope through one longitudinal mode and the total number of screen divisions corresponding to this mode were noted. This allowed calibration of the oscilloscope's horizontal axis since it is known that the cavity frequency interval between any two adjacent longitudinal laser modes is given by $c/2L$. The calibration factor was calculated to be 8.4 MHz/cm.

When the output of laser 1 was unblocked and directed through the cell, there was a dramatic increase in the transmission of the medium in the spectral vicinity of the saturating beam. A typical sweep of the hole is shown in Figure 12. The oscillograph was made by use of multiple exposure; several successive sweeps were photographed with laser 1 blocked and then unblocked.

In order to more accurately probe the medium, it was found necessary to reduce the level of laser 2 to a smaller intensity than was used to obtain the oscillograph of Figure 12. This was necessary to insure that the intensity of laser 2 was much less than the saturation intensity, which was assumed in the theory of section 2.2.3. The reduced signal level required the use of synchronous detection to give a usable display.
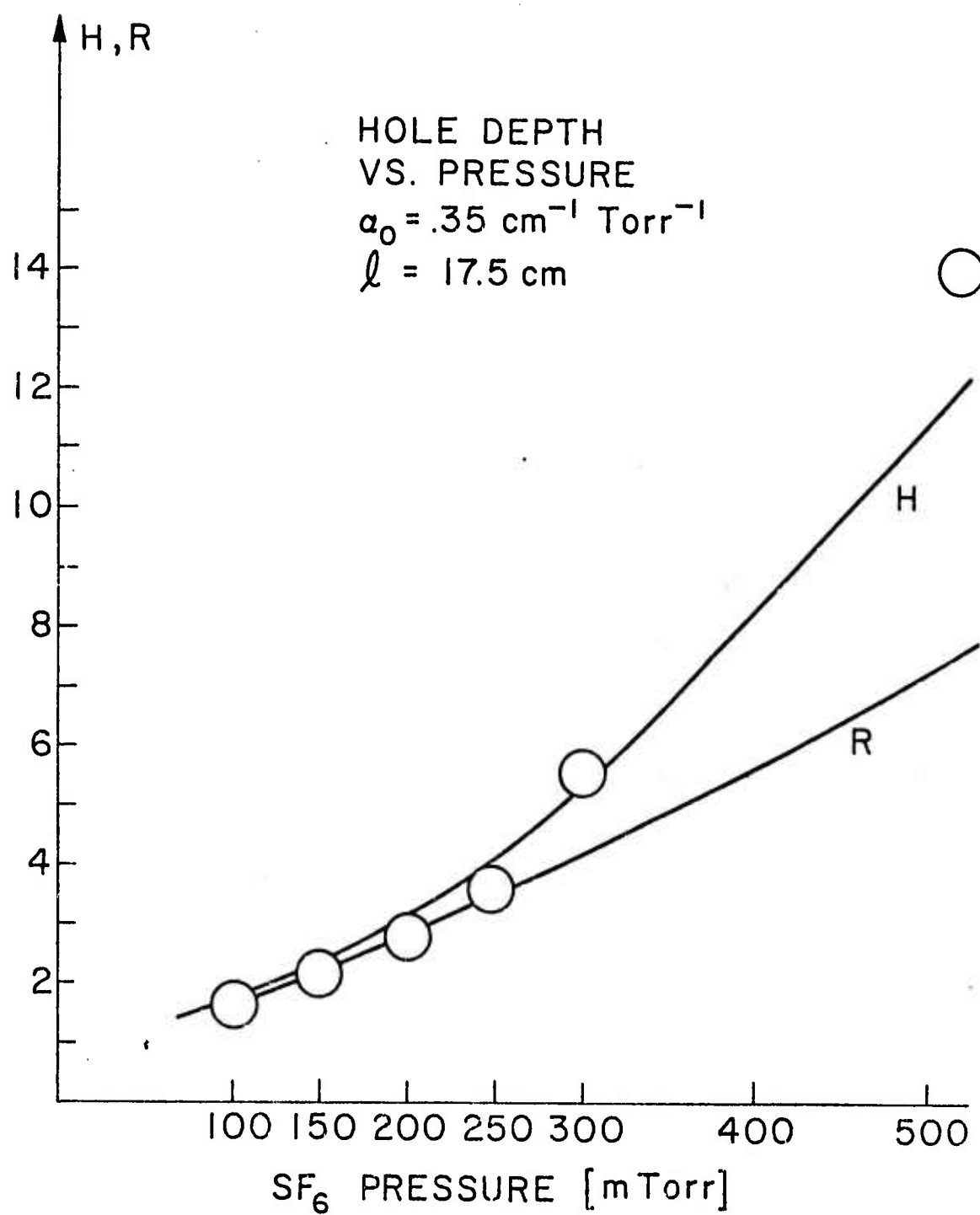
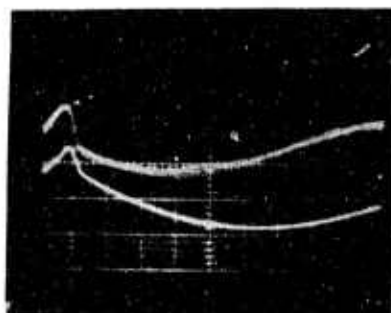Fig. 10 Hole Depth vs. Pressure

Fig. 11 Swept P(18) laser mode. Upper trace: Absorber cell evacuated. Lower trace: SF_6 pressure 300 mTorr. (Hor.: approx. 5 MHz/div.)
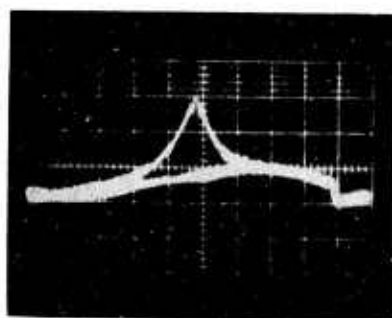
Fig. 12 A Typical Hole. Transmission of the absorber is increased due to saturation of the medium by laser 1. Note presence of beat note. (Hor.: approx. 5 MHz/div.)

The pressure in the SF$_6$ cell was set to various pressures in the range 100 to 500 mTorr. and the unfiltered output of the lock-in amplifier was displayed on the oscilloscope and recorded photographically. In each case, the minimum test-beam intensity was used. The results of this procedure are shown in Figure 13.

The full width at half maximum (FWHM) of the holes shown in Figure 13 were measured and are shown plotted in Figure 14. The width remains essentially constant (within experimental error) over the pressure range indicated in agreement with the theory of section 2.2.3 (see Figure 6). Comparison of the theoretical curves with the measured FWHM allows an estimate to be made of the pressure-broadening coefficient, K_{pb}. The measured FWHM remains approximately constant at $\approx$ 12 MHz. As seen in Figure 6, this corresponds to a frequency deviation of $\approx$ 12 (in muitiples of $K_{pb}/10$). The pressure-broadening coefficient is then

$$K_{pb} \approx \frac{(12 \text{ MHz.}) (10)}{(12)} = 10 \text{ MHz/Torr} .$$

This agrees closely with the values reported previously[1, 5].

The conclusions of this study and recommendations for further work are given in Section 5.

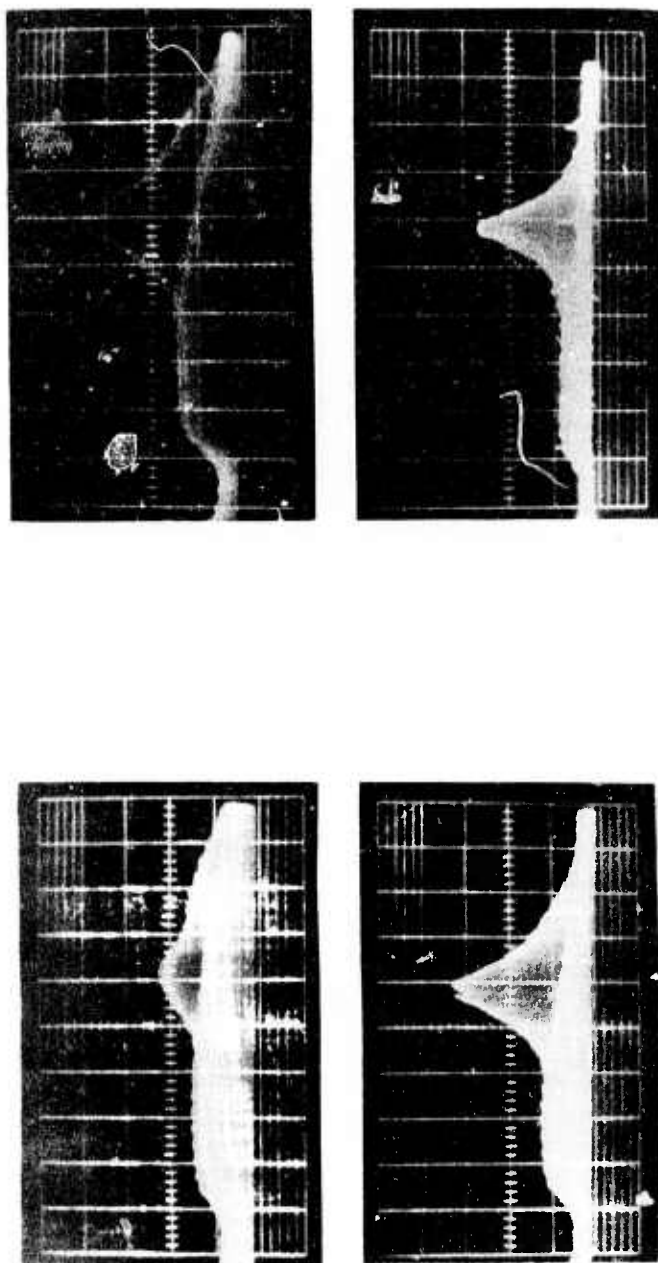Fig. 13 Oscillographs showing hole shapes. The power level of the saturating beam was maintained at 140 mW. The pressure was (left to right, top to bottom) 150, 250, 300, and 500 mTorr respectively. (Hor.: 8.4 MHz/div.)
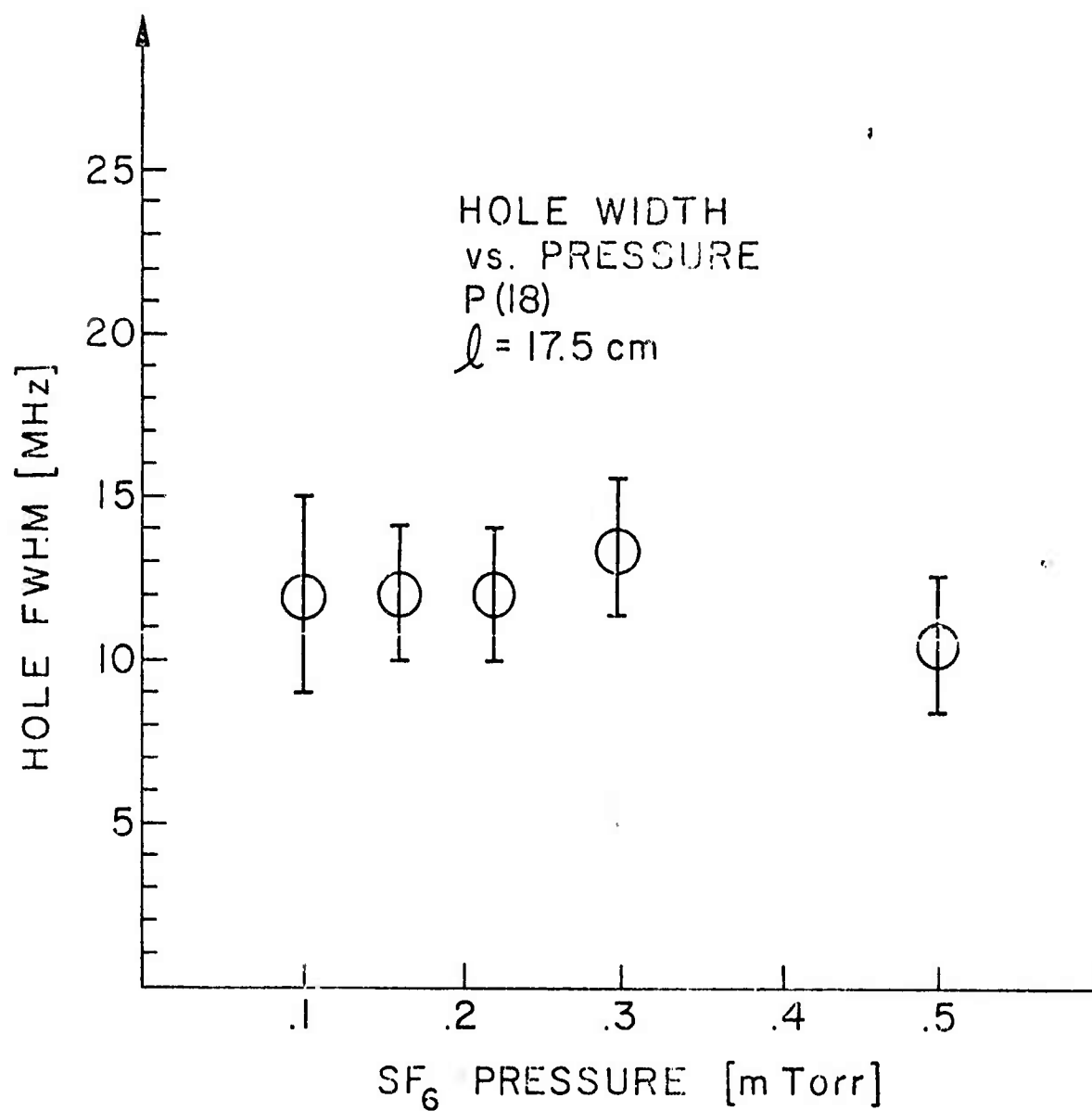
Fig. 14 Hole Width (FWHM) vs. Pressure

3.0 EXPERIMENTAL STUDY OF A XENON-XENON BALAD RECEIVER SYSTEM

The equipment which has been assembled for this study includes two He-Xe lasers, a pure xenon discharge absorption cell, assorted optical elements for directing and modifying the laser output beams, and both liquid N_2 cooled Ge:Au detectors and room temperature InAs detectors. The shorter of the two lasers has an active discharge length of 26 cm and a 5 mm inside diameter. The longer laser, which can alternatively be used as a laser amplifier, has an active length of 69 cm and a 10 mm I.D. The lasers were at times operated with a "standard" low-loss laser resonator geometry with transmission output coupling and an intra-cavity aperture to restrict laser oscillation to the fundamental mode. A higher output power was generally achieved using "diffraction output coupling"[11]. In the latter case, one mirror of the laser resonator consists of a small (e.g., 1 mm diameter) gold dot supported on a quartz substrate. The useful output in this geometry consists of the ordinary "diffraction loss" which is coupled around the small dot reflector. Both lasers are excited with aluminum cold cathodes. A non-excited cathode to anode return path is provided to reduce density gradients due to cataphoresis.

Two absorber cells have been investigated: One with a 10 mm I.D. and 11 cm discharge length[1] and another with a 5 mm I.D. and a 20 cm discharge length. In order to operate a high current discharge at low pressures of pure Xenon without excessive sputtering, thermionic cathodes were used in both absorption cells. Xenon cleanup was significant, and stable operation which yielded reproducible results at the lower pressures could be achieved only after continually adding more xenon to the absorption cell. The use of a solid xenon reservoir at an adjustable temperature[12] could help overcome this difficulty. The comparison of the two absorption cells indicates that the optimum operating conditions to achieve the maximum absorption scales in the same manner as the optimum conditions for maximum gain in the laser discharge. That is, the 5 mm I.D. cell yielded twice the maximum absorption coefficient as the 10 mm I.D. cell (α = 60 dB/m) and the maximum occurred for twice the pressure (100 mTorr) and half the total current (50 mA). It has been difficult to achieve noise-free operation of the xenon discharges, particularly in the pure xenon discharge of the absorbers.

The detailed description of the experiments and the experimental results will be reported in the final report.

4.0 THEORETICAL STUDY OF THE PROPAGATION OF OPTICAL PULSES WITH LIMITED TRANSVERSE EXTENT IN SATURATED ABSORBERS

The computer program which describes the propagation of a coherent optical pulse in a resonant medium has been extended to the three dimensions with cylindrical symmetry as suggested previously[1].

Preliminary results indicate the existence of a self-focusing effect. That is, an initially collimated wave (with finite transverse extent) is brought to a focus. The work is progressing and the complete description of the problem and the experimental results will be presented in the final report.

It should be noted, that if such a self-focusing effect exists and can be verified experimentally, it may be possible to guide the amplified, coherent signal in the BALAD receiver by this means, and achieve attenuation of background and spontaneous emission noise by means of spatial filtering, rather than having to depend on "brute force" attenuation in the saturable absorber. The details of this possible design modification will be discussed in the final report.

5.0 CONCLUSIONS AND RECOMMENDATIONS

1. The spatial filtering capability of a SF_6 absorber in a BALAD receiver configuration has not been experimentally verified, as well as the frequency domain filtering capability.

5.1 The experimental study has specifically demonstrated that the free-focus configuration of the BALAD receiver using sulfur hexafluoride can be used to filter wideband and wide-angle noise from a narrow-band optical signal from an unresolved source. The angular selectivity of such a system is approximately equal to the resolving power of the collection optics for an appropriately designed absorber configuration.

Relative noise attenuations on the order of 10 db. have been demonstrated and higher attenuations can be obtained through optimization and the cascading of several such cells.

The attenuation suffered by the noise which is approximately coherent with the signal is affected by a parametric process similar to the so-called "MARS" amplification.

Areas in which further research would be desirable include the extent to which attenuation is dependent on polarization, the effect of diffusion at much lower pressures and smaller spot diameters, the effect of thermal gradients within the absorber, the effect of parametric processes on noise coherent with the signal, and alternate structures to prevent the beam from respreading.

2. The xenon-xenon system is assembled and the experimental test of that BALAD system is in progress. Difficulties have been encountered in maintaining low noise operation of the xenon discharges. This task is continuing and results will be reported in the final report.

3. A self-focusing effect has been uncovered in the theoretical study of the propagation of optical pulses in a resonant absorber in three dimensions. If this effect can be verified experimentally, an improvement in the design and performance of the BALAD receiver may be possible. This task is continuing and results will be reported in the final report.

References

1. G. Gould and J. T. LaTourrette, "Bleachable Absorber Laser Amplifier and Detector," RADC TR-72-313, October 1972.

2. J. Wilson, "Investigation of the Use of a Saturable Absorber in a Low-Noise, Wide-Angle Laser Receiver," Master of Science Thesis, Electrophysics Department, Polytechnic Institute of Brooklyn, June 1973.

3. W. Smith and P. Sorokin, "The Laser," McGraw-Hill, New York, 1966.

4. H. Brunet and M. Perez, "The ν_3 and ν_4 Bands of Sulfur Hexafluoride," J. Mol. Spectroscopy, 29, (1969).

5. P. Rabinowitz, "Lamb Dip Spectroscopy and CO_2 Frequency Stabilization on SF_6," AFOSR 70-2004TR, June 1970.

6. A. Yariv, "Quantum Electronics," John Wiley and Sons, New York, 1967.

7. W. Rigrod, "Gain Saturation and Output Power of Optical Masers," J. Appl. Physics, 34, p. 2602, (1963).

8. B. Senitzky and S. Cutler, "Amplification by Resonance Saturation in Millimeter Wave Cavities," Microwave Journal, January 1964.

9. A. Carlson, "Communication Systems," pp. 159-160, McGraw-Hill, New York 1968.

10. Weast, "Standard Mathematical Tables," pp. 396-397, Chemical Rubber Company, Cleveland, 1968.

11. J. T. LaTourrette, S. F. Jacobs, and P. Rabinowitz, "Improved Laser Angular Brightness Through Diffraction Coupling," Appl. Optics 3, 981, (1964).

12. D. R. Armstrong, "A Method for the Control of Gas Pressure in Xenon Laser," IEEE J. of Quantum Electronics, Vol. 4, Nov. 1968, pp. 968-969.

APPENDIX A

Integration of Equations (5) and (37)

The propagation of a monochromatic plane wave through an inhomogeneously broadened medium is given by equation (5) or

$$-\alpha_o dz = \int \frac{(1 + s)^{\frac{1}{2}}}{s} ds \qquad (A1)$$

which integrates to

$$-\alpha_o \ell = \int_{s_1}^{s_2} \frac{(1 + s)^{\frac{1}{2}}}{s} ds = A(s) \Big|_{s_1}^{s_2} \qquad (A2)$$

where ℓ is the length of the absorber

   s is the normalized intensity

   α_o is the unsaturated absorption coefficient.

Using the substitution $w = (1 + s)^{\frac{1}{2}}$

$$A(s) = \int \frac{(1 + s)^{\frac{1}{2}}}{s} ds = \int \frac{2w^2}{w^2 - 1} dw = \int \left(\frac{w}{w + 1} + \frac{w}{w - 1} \right) dw . \qquad (A3)$$

Letting $v_1 = w + 1$ and $v_2 = w - 1$

$$A(s) = \int \frac{v_1 - 1}{v_1} dv_1 + \int \frac{v_2 + 1}{v_2} dv_2 = \int dv_1 + \int dv_2 - \int \frac{dv_1}{v_1} + \int \frac{dv_2}{v_2} \qquad (A4)$$

$$= (v_1 + v_2) + \ln \left(\frac{v_2}{v_1} \right) . \qquad (A5)$$

Substituting back for s

$$A(s) = 2(1 + s)^{\frac{1}{2}} + \ln \left[\frac{(1 + s)^{\frac{1}{2}} - 1}{(1 + s)^{\frac{1}{2}} + 1} \right] \qquad (A6)$$

which can be rearranged to

$$A(s) = \ln s + 2(1 + s)^{\frac{1}{2}} - 2 \ln \left[(1 + s)^{\frac{1}{2}} + 1 \right] \qquad (A7)$$

37

The propagation of a small-signal field at frequency ν through a saturable absorber in which a "hole" has been burned by a saturating field at frequency ν_o is described by equation (37), or

$$\frac{du}{u} = \left[\frac{((1+s)^{\frac{1}{2}} + 1)^2 + \delta^2 (1+s)^{\frac{1}{2}}}{((1+s)^{\frac{1}{2}} + 1)^2 + \delta^2} \right] \frac{ds}{s} \tag{A8}$$

where δ is the frequency difference normalized to the homogeneous half-width.

Equation (A8) integrates to

$$u_2 = u_1 \exp \left\{ \phi(s_2) - \phi(s_1) \right\} \tag{A9}$$

where

$$\phi(s) = \int \left[\frac{((1+s)^{\frac{1}{2}} + 1)^2 + \delta^2 (1+s)^{\frac{1}{2}}}{((1+s)^{\frac{1}{2}} + 1)^2 + \delta^2} \right] \frac{ds}{s} \; . \tag{A10}$$

Using the substitution $w = (1+s)^{\frac{1}{2}}$

$$\phi(w) = \int \frac{(w+1)^2 + \delta^2 w}{(w+1)^2 + \delta^2} \left[\frac{2w}{w^2 - 1} \right] dw \; . \tag{A11}$$

With the benefit of equation (A6) and some hindsight, a trial solution is assumed of the form

$$\phi(s) = \ln \left[\frac{(1+s)^{\frac{1}{2}} - 1}{(1+s)^{\frac{1}{2}} + 1} \right] + g(s) \tag{A12}$$

or

$$\phi(w) = \ln \frac{(w-1)}{(w+1)} + g(w) \; . \tag{A13}$$

Differentiating

$$\phi'(w) = \frac{(w+1)}{(w-1)} \left[\frac{w+1-w+1}{(w+1)^2} \right] + g'(w) \; . \tag{A14}$$

Using equation (A11),

$$g'(w) = \left(\frac{2w}{w^2 - 1} \right) \left[\frac{(w+1)^2 + \delta^2 w}{(w+1)^2 + \delta^2} \right] - \left(\frac{2}{w^2 - 1} \right). \tag{A15}$$

Equation (A15) can be written as

$$g'(w) = \frac{2w + 2(1 + \delta^2)}{P(w)} \tag{A16}$$

38

where $P(w) = (w + 1)^2 + \delta^2$.

Integrating

$$g(w) = 2 \int \frac{w}{P(w)} \, dw + 2(1 + \delta^2) \int \frac{dw}{P(w)} . \tag{A17}$$

The integrals may be evaluated using a table of integrals[10]

$$g(w) = 2 \left[\frac{1}{2} \ln P(w) - \frac{dw}{P(w)} \right] + 2 \int \frac{dw}{P(w)} + 2\delta^2 \int \frac{dw}{P(w)} . \tag{A18}$$

$$g(w) = \ln P(w) + 2\delta^2 \int \frac{dw}{P(w)} \tag{A19}$$

$$= \ln P(w) + 2\delta \tan^{-1} ((w + 1)/\delta) . \tag{A20}$$

The function $\phi(w)$ is then given by

$$\phi(w) = \ln \frac{(w - 1)}{(w + 1)} \ln ((w + 1)^2 + \delta^2) + 2\delta \tan^{-1} \left[\frac{w + 1}{\delta} \right]. \tag{A21}$$

Equation A(21) can be rearranged to yield

$$\phi(w) = \ln s + \ln \left[\frac{(w + 1)^2 + \delta^2}{(w + 1)^2} \right] + 2\delta \tan^{-1} \left[\frac{(w + 1)}{\delta} \right]. \tag{A22}$$

Equation (A22) is the result cited in equation (39).

39

APPENDIX B
Computer Programs

This Appendix contains the programs used to obtain various numerical results used in this report. The programs are as follows:

1. <u>BALAD I</u>. Used to evaluate the Attenuation function, $A(s)$, for values of s in the range of $0.1 \leq s \leq 500$. The results are shown plotted in Figure 4.

2. <u>HOLEDEEP</u>. Used to evaluate the "real" hole depth, R, and the "apparent" hole depth, H, as given by equations (8) and (19) respectively. The results are shown plotted in Figure 10.

3. <u>TRY</u>. Used to evaluate the small-signal attenuation (linear model) as given by equations (38) and (39).

The programs are written in PLAGO, a compatible version of PL/I. They were processed on an IBM System 370 Computer.

```
$BEGIN

P L A G O        VERSION 2. 20

  STMT BLK NEST

        0              BALADI:PROC OPTIONS(MAIN);
        1              DECLARE N1(4), N3(4), D(4);
        2              N1=1.1;
        3              N2=101;
        4              N2(4)=51;
        5              PUT SKIP LIST('S IS NORMALIZED INTENSITY');
        6              PUT SKIP (2) (LIST('S', 'S(DB)', ' F(S)', ' FN(S)');
        7              MLOOP:DO M = 1 TO 4;
        8       1      D(M)=10. **(3-M);
        9       1      JLOOP:DO J = N1(M) TO N2(M);
       10       2      B=J-1;
       11       2      S= B/D(M);
       12       2      RT=SQRT(1. +S);
       13       2      F=2*RT+LOG((RT-1)/(RT+1));
       14       2      FN= F-(2. -LOG(4));
       15       2      DB= 10. *LOG10(S);
       16       2      PUT SKIP LIST(S, DB, F, FN);
       17       2      END JLOOP;
       18       1      PUT SKIP(2);
       19       1      END MLOOP;
       20              END BALADI;

$DATA

$END
```

$BEGIN

P L A G O   VERSION 2.20

```
STMT BLK NEST                        TEXT

   0              HOLEDEEP:PROC OPTIONS (MAIN);
   1              DECLARE P(6);
   2              P(1)=.1;P(2)=.15;P(3)=.2;P(4)=.25;P(5)=.3;P(6)=.5;
   8              JLOOP:DO J = 1 TO 6;
   9        1     SN=3.12/(P(J)**2);
  10        1     PR=P(J);
  11        1     AL=17.5*.35*P(J);
  12        1     RT= SQRT(1+SN);
  13        1     AF=LOG(SN) +2*RT-2*LOG(RT+1);
  14        1     AOUT=AF-AL;
  15        1     SGS=SN/2.;
  16        1     KLOOP:DO K= 1 TO 5;
  17        2     RTG=SQRT(1+SGS);
  18        2     C=LOG(SGS)+2*RTG-2*LOG(RTG+1)-AOUT;
  19        2     C=(C*SGS)/RTG;
  20        2     SGS=SGS-C;
  21        2     PUT LIST(SGS);
  22        2     END KLOOP;
  23        1     H=(SGS/SN)*EXP(AL);
  24        1     HAPP=H*SQRT((1+SN)/(1+SGS));
  25        1     PUT SKIP LIST        ('PRESSURE=',PR);
  26        1     PUT SKIP LIST        ('           AL=',AL);
  27        1     PUT SKIP LIST ('         H=',H);
  28        1     PUT SKIP LIST ('H APPARENT=',HAPP);
  29        1     PUT SKIP LIST('S IN=',SN);
  30        1     PUT SKIP LIST        ('S OUT=',SGS);
  31        1     PUT SKIP(4);
  32        1     END JLOOP;
  33              PUT PAGE;
  34              END HOLEDEEP;
```

$BEGIN

P L A G O   VERSION 2. 20

```
STMT BLK NEXT                    TEXT
   0              TRY:PROC OPTIONS(MAIN);
   1              DECLARE LINE CHAR(120);
   2              LINE=(120)'*';
   3              PUT SKIP LIST(LINE);
   4              PUT SKIP(4)LIST('FREQ DEV IS IN MULTIPLES OF PBF/10');
   5              ILOOP:DO I = 1 TO 20;
   6        1     GET LIST(SN, P);
   7        1     G=0. 2/P;
   8        1     AL= 17. 5*. 35*P;
   9        1     PUT SKIP(4) LIST(LINE);
  10        1     PUT SKIP(2) LIST('PRESSURE=', P);
  11        1     PUT SKIP LIST('AL=', AL);
  12        1     PUT SKIP LIST('S IN =', SN);
  13        1     C=ATT(SN);
  14        1     S=SN*EXP(-AL);
  15        1     KLOOP:DO K= 1 TO 8;
  16        2     S=S- ((ATT(S)+AL-C)*S/SQRT(1+S));
  17        2     END KLOOP;
  18        1     PUT SKIP LIST('S OUT =', S);
  19        1     PUT SKIP(2) LIST('  FREQ DEV','S. S. ATTEN.','ATTEN,
                  NORM.');
  20        1     JLOOP:DO J= 0 TO 20;
  21        2     DELTA=J;DELTA=DELTA*G;
  23        2     A=BAND(S, DELTA)/ BAND(SN. DELTA);
  24        2     IF J=0 THEN AMAX=A;
  26        2     AREL=A/AMAX;
  27        2     PUT SKIP LIST(J, A, AREL);
  28        2     END JLOOP;
  29        1     A=EXP(-AL);
  30        1     AREL=A/AMAX;
  31        1     PUT SKIP LIST('    INFINITY', A, AREL);
  32        1     END ILOOP;
  33              GO TO FIN;
  34              ATT:PROC(X);
  35    1   1     RT=SQRT(1+X);
  36    1   1     F= 2*RT+LOG(X)-2*LOG(RT+1);
  37    1   1     RETURN(F);
  38    1   1     END;
  39              BAND:PROC(X, D);
  40    1   1     RT=SQRT(1+X);
  41    1   1     RPW=RT+1;
  42    1   1     T=0;  IF D=0 THEN GO TO FS;
  45    1   1     T=2*D*ATAN(RPW/D);
  46    1   1     FS:F= X*(RPW**2+D**2)*EXP(T);
  47    1   1     F=F/(RPW**2);
  48    1   1     RETURN(F);
  49    1   1     END;
  50              FIN:END TRY;
```

43

Signal to Noise Ratio Calculations

The effect of a saturable absorber on the detected signal to noise ratio (S/N) is calculated* for two cases: noise which is approximately coherent with the signal, and totally incoherent noise.

CASE 1:   Coherent noise

Narrowband random noise can be represented by in-phase and quadrature components[9].

$$E = E_o \cos \omega_o t + n_c(t) \cos \omega_o t + n_s(t) \sin \omega_o t \tag{A23}$$

where E_o is the signal field amplitude and

$n_c(t)$, $n_s(t)$ are the in-phase and quadrature noise components respectively and have independent, zero-mean gaussian distributions.

The intensity of the field is then

$$I(t) = E^2 = (E_o + n_c)^2 \cos^2 \omega_o t + n_s^2 \sin^2 \omega_o t$$
$$2(E_o + n_c)n_s \sin \omega_o t \cos \omega_o t \tag{A24}$$

When equation (A24) is simplified, integrated over a time long compared to the optical period, and only first-order terms retained (this assumes n_c and n_s are small compared to E_o), the result is

$$\overline{I} \cong \frac{E_o^2}{2} + E_o n_c(t). \tag{A25}$$

Normalizing to the saturation intensity, I_s, yields

$$s \equiv \frac{\overline{I}}{I_s} = \frac{E_o^2}{2I_s} + \frac{E_o n_c(t)}{I_s} \equiv s + \Delta s(t). \tag{A26}$$

When the field is incident on a photodetector, it gives rise to signal and noise currents given by

$$i_s = K_d I_s s$$
$$\tag{A27}$$
$$i_n = K_s I_s \Delta s(t).$$

---

*This treatment neglects all noise sources other than spontaneous emission noise and background noise.

The detected signal to noise ratio (power ratio is then

$$(S/N)_{det} = \frac{\overline{i_s^2}}{\overline{i_n^2}} = \frac{I_s^2 K_d^2}{I_s^2 K_d^2} \left(\frac{s^2}{\Delta s^2} \right) . \qquad (A28)$$

From equation (22)

$$\frac{s_2}{\Delta s_2} = \frac{s_1}{\Delta s_1} \cdot \left(\frac{R}{H} \right) . \qquad (A29)$$

Therefore

$$(S/N)_2 = (S/N)_1 \, (R^2/H^2) . \qquad (A30)$$

CASE 2:   Totally Incoherent Noise

In this case, no heterodyning of the noise with the signal is present, since the two fields are incident on physically distinct areas of the detector, or have a frequency difference outside the detector bandwidth, or both. Only fluctuations in the total optical noise power are seen at the detector. The mean-square fluctuation of the intensity of the noise field, falling within the detector bandwidth Δf, are given by[20]

$$\overline{I^2(t)} = \frac{1}{2} \frac{\Delta f}{\Delta \nu} P_n^2 \qquad (A31)$$

where $\Delta \nu$ is the noise bandwidth

P_r is the total noise power.

This gives rise to a photodetector noise current, i_n

$$\overline{i_n^2} = \frac{K_d^2 \, \Delta f}{2 \, \Delta \nu} \left(P_n^2 \right) . \qquad (A32)$$

The signal current is

$$i_s = K_d P_s \qquad (A34)$$

where P_s is the signal power (optical).

The signal to noise ratio is then

$$(S/N) = \frac{\overline{i_s^2}}{\overline{i_n^2}} = \frac{K_d^2}{K_d^2 \Delta f / 2 \Delta \nu} \frac{P_s^2}{P_n^2} = (\text{const}) \frac{P_s^2}{P_n^2} \qquad (A35)$$

In traveling through the saturable absorber, the signal intensity (power) is attenuated by

$$\frac{P_{s2}}{P_{s1}} = R \exp(-\alpha_o \ell) \qquad (A36)$$

while the noise is attenuated by

$$\frac{P_{n2}}{P_{n1}} = \exp(-\alpha_o \ell). \qquad (A37)$$

Combining equations (A35), (A36) and (A37) yields

$$(S/N)_2 = (S/N)_1 \, (R^2) \qquad (A38)$$